CXXC-finger protein 1 associates with FOXP3 to stabilize homeostasis and suppressive functions of regulatory T cells

Xiaoyu Meng, [1,2,3†] Yezhang Zhu, [4,5 †] Kuai Liu, [1,2,3 †] Yuxi Wang,[6] Xiaoqian Liu, [1,2,3] Chenxin Liu,[2] Yan Zeng, [1,2,3] Shuai Wang, [1,2,3] Xianzhi Gao, [1,2,3] Xin Shen, [7] Jing Chen, [8] Sijue Tao, [6] Qianying Xu, [2] Linjia Dong, [9] Li Shen, [10,11,*] and Lie Wang[1,2,3,6,12,**]

[1]Institute of Immunology and Bone Marrow Transplantation Center, The First Affiliated Hospital, Zhejiang University School of Medicine, Hangzhou, China.

[2]Zhejiang University School of Medicine, Hangzhou, China.

[3]Liangzhu Laboratory, Zhejiang University Medical Center, Hangzhou, China.

[4]Department of Hematology, Tongji Hospital, School of Medicine, Tongji University, Shanghai, China

[5]Shanghai Key Laboratory of Signaling and Disease Research, Frontier Science Center of Stem Cell Research, National Stem Cell Translational Resource Center, School of Life Sciences and Technology, Tongji University, Shanghai, China

[6]Laboratory Animal Center, Zhejiang University, Hangzhou, China.

[7]Co-Facility Center, Zhejiang University School of Medicine, Hangzhou, China

[8]Department of Gastrointestinal Surgery, The Second Affiliated Hospital, Zhejiang University School of Medicine, Hangzhou, China.

[9]School of Basic Medical Sciences and Forensic Medicine, Hangzhou Medical College, Hangzhou, China

[10]MOE Key Laboratory of Biosystems Homeostasis & Protection and Zhejiang Provincial Key Laboratory for Cancer Molecular Cell Biology, Life Sciences Institute, Zhejiang University, Hangzhou, China.

[11]Department of Orthopedics Surgery, the Second Affiliated Hospital, School of Medicine, Zhejiang University, Hangzhou, China

[12]Future Health Laboratory, Innovation Center of Yangtze River Delta, Zhejiang University, Jiaxing, China.

[†] These authors contributed equally to this work.

* Correspondence: wanglie@zju.edu.cn; li_shen@zju.edu.cn.

Abstract

FOXP3-expressing regulatory T (T_{reg}) cells play a pivotal role in maintaining immune homeostasis and tolerance, with their activation being crucial for preventing various inflammatory responses. However, the mechanisms governing the epigenetic program in T_{reg} cells during their dynamic activation remain unclear. In this study, we demonstrate that CXXC finger protein 1 (CXXC1) interacts with the transcription factor FOXP3 and facilitates the regulation of target genes by modulating H3K4me3 deposition. *Cxxc1* deletion in T_{reg} cells leads to severe inflammatory disease and spontaneous T-cell activation, with impaired immunosuppressive function. As a transcriptional regulator, CXXC1 promotes the expression of key T_{reg} functional markers under steady-state conditions, which are essential for the maintenance of T_{reg} cell homeostasis and their suppressive functions. Epigenetically, CXXC1

binds to the genomic regulatory regions of T_{reg} program genes in mouse T_{reg} cells, overlapping with FOXP3 binding sites. Given its critical role in T_{reg} cell homeostasis, CXXC1 presents itself as a promising therapeutic target for autoimmune diseases.

Introduction

Regulatory T (T_{reg}) cells are a distinct subset of $CD4^+$ T cells that play a critical role in maintaining immune homeostasis and self-tolerance by suppressing excessive or aberrant immune responses to foreign or self-antigens [1-3]. These cells can be further categorized into thymus-derived regulatory T cells (tT_{reg} cells), periphery-derived T_{reg} cells (pT_{reg} cells), and induced T_{reg} cells (iT_{reg} cells) [4]. They uniquely express the transcription factor FOXP3, a member of the forkhead winged-helix family, which is essential for T_{reg} cell lineage commitment and suppressive function [5,6]. Deletion or mutation of the *Foxp3* gene leads to a range of immunological disorders, including allergies, immunopathology, and autoimmune diseases in both mice and humans [7,8].

It is well established that FOXP3 recruits various cofactors to form complexes that either promote or repress the expression of downstream genes, with histone and DNA modifications playing pivotal roles in this process. FOXP3 can activate or repress the transcription of key regulators of T_{reg} cell activation and function by recruiting the histone acetyltransferases (HATs) or histone deacetylases (HDACs)[9,10]. Notably, FOXP3-bound sites exhibit enrichment of H3K27me3, a modification essential for FOXP3-mediated repressive chromatin remodeling under inflammatory conditions[11]. However, the direct role of FOXP3 as a transcriptional activator through interactions with epigenetic regulators, particularly via

modulation of H3K4 trimethylation, remains poorly documented.

In mammals, six proteins have been identified that catalyze H3K4 methylation. These proteins contain the SET domain and include MLL1 (KMT2A), MLL2 (KMT2B), MLL3 (KMT2C), MLL4 (KMT2D), SETD1A, and SETD1B [12,13]. For example, MLL1 plays a critical role as an epigenetic regulator in T_{reg} cell activation and functional specialization[14]. Additionally, Placek *et al.* demonstrated that MLL4 is essential for T_{reg} cell development by catalyzing H3K4me1 at distant unbound enhancers through chromatin looping [15]. H3K4me3, which is enriched at the transcription start site (TSS) and the CpG island (CGI), converts chromatin into active euchromatin by recruiting activating factors [16]. CXXC finger protein 1(CXXC1, also known as CFP1), which contains a SET1 interaction domain (SID), is required for binding to the histone H3K4 methyltransferases SETD1A and SETD1B [17]. Previous studies have shown that CXXC1 regulates promoter patterns during T cell maturation, GM-CSF-derived macrophage phagocytosis, TH17 cell differentiation, and the function of ILC3 cells with aging by modulating H3K4me3 modification[18-21]. Despite the well-documented role of CXXC1 in various immune effector cells, its role in T_{reg} cells remains unclear.

Here, we demonstrate that CXXC1 interacts with FOXP3 and enhances the expression of FOXP3 target genes. T_{reg} cell-specific deletion of *Cxxc1* triggers systemic autoimmunity, accompanied by multiorgan inflammation, ultimately resulting in early-onset fatal inflammatory disease in mice. *Cxxc1*-deficient T_{reg} cells exhibit a disadvantage in proliferation and homeostasis, even in non-inflammatory mice where coexisting wild-type (WT) T_{reg} cells were present. Moreover, *Cxxc1*-deficient T_{reg} cells display intrinsic defects in

the expression of key suppression molecules, including CTLA-4, CD25, ICOS, and GITR. Consistent with these findings, mechanistic studies strongly suggest that CXXC1 functions as an essential cofactor of FOXP3, playing a crucial role in sustaining H3K4me3 modifications at key T_{reg} cell genes.

Materials and Methods

Mice

All mice used in this study were bred for a minimum of seven generations on a C57BL/6 background. Mouse experiments, or cells from mice of the same genotype, compared littermates or age-matched control animals. The *Cxxc1*$^{fl/fl}$ mouse strain has been previously described [22]. The *Foxp3*^{cre} mice (JAX,016959) were generously provided by Bin Li (Shanghai Jiao Tong University School of Medicine, Shanghai, China). CD45.1 (NM-KI-210226) mice were purchased from the Nanjing Biomedical Research Institute of Nanjing University. *Rag1*$^{-/-}$ mice (stock#T004753) were purchased from GemPharmatech. 2D2 (MOG35-55-specific TCR transgenic) mice were graciously supplied by Prof. Linrong Lu (Zhejiang University School of Medicine, Hangzhou, Zhejiang, China). *Foxp3*^{cre} (WT) and *Foxp3*^{cre} *Cxxc1*$^{fl/fl}$ (cKO) were utilized at 3 weeks old unless otherwise stated. All mice were housed in the Zhejiang University Laboratory Animal Center under specific pathogen-free conditions, and all animal experimental procedures were approved by the Zhejiang University Animal Care and Use Committee (approval no.ZJU20230246).

Cell culture

HEK 293T cells were obtained from ATCC, and Plat E cells were kindly provided by Prof. Xiaolong Liu (Shanghai Institutes for Biological Sciences). Both cell lines were cultured in Dulbecco-modified Eagle medium (DMEM) containing 10% (v/v) fetal bovine serum (FBS), supplemented with 1% penicillin/streptomycin.

Immunofluorescence (IF) Staining

As previously described [23], coverslips were treated with a 0.01% poly-L-lysine solution (P4707; Sigma) for 10 minutes, air-dried, and then coated with $CD4^+$ YFP^+ T_{reg} cells. The cells were then fixed in 4% formaldehyde for 15 minutes at room temperature, permeabilized with 0.2% Triton X-100, and blocked with 1% BSA. Antibodies against CXXC1 (ab198977; Abcam) and FOXP3(17-5773-82; Invitrogen) were diluted in Image iT FX signal enhancer (I3693; Invitrogen) and incubated with cells overnight at 4 °C. After washing with phosphate-buffered saline (PBS), the cells were incubated with a goat anti-rabbit antibody Alexa Fluor 594 (1:250;10015289; Invitrogen) secondary antibody and stained with DAPI (200 ng/mL; D523; Dojindo). Slides were washed with PBS and sealed with an antifade solution(P36934; Invitrogen) before imaging with an Olympus FV3000 fluorescence microscope. The images were visualized using the FV31-SW software.

Co-immunoprecipitation and western blot

Harvest the appropriate transfected cell lines and primary cells from culture and wash them with ice-cold PBS. Lyse the cells in NETN300 buffer (300 mM NaCl, 0.5 mM EDTA,

0.5% (v/v) NP-40, 20 mM Tris-HCl pH 8.0) supplemented with a protease inhibitor (1:100, P8340, Sigma-Aldrich) and PMSF (1 mM) on ice for 10 minutes. Take a small portion of the whole-cell lysate as input, and incubate the remaining lysate with either Anti-FLAG M2 Beads (M8823; Sigma) or Anti-HA Beads (HY-K0201; MCE) on a rotator at 4°C overnight. For the endogenous Co-IP assay targeting CXXC1 and FOXP3, incubate the cell lysate with protein G magnetic beads along with anti-CXXC1 (ab198977; Abcam) or anti-FOXP3 (14-4774-82; Invitrogen) antibodies on a rotator at 4°C overnight. Wash the beads three times with IP buffer (100 mM NaCl, 0.5 mM EDTA, 0.5% (v/v) NP-40, 20 mM Tris-HCl pH 8.0) to remove non-specific binding. Boil the washed beads with 1× Laemmli sample buffer (1610747; Bio-Rad) to elute the bound proteins. Separate the denatured proteins by SDS-PAGE. Transfer the separated proteins onto PVDF membranes (Millipore) for immunoblotting.Immunoblot the PVDF membranes (IPVH00010) with the following antibodies: anti-CXXC1 (1:1000; ab198977; Abcam), anti-FOXP3 (1:500; 14-7979-80; Invitrogen), anti-FlAG (1:1000; 14793; Cell Signaling Technology), anti-HA (1:1000; 3724S; Cell Signaling Technology).Detect the immunoblotted proteins using a secondary HRP-conjugated goat anti-rabbit antibody (1:1000; HA1001-100; Huabio) and visualize the bands using an appropriate detection method.

ELISA

Serum samples from 3-week-old WT and KO mice were analyzed for total IgG and IgE concentrations using ELISA kits (88-50630-88; eBioscience) according to the manufacturer's instructions. Half-area ELISA plates were coated with Coating Buffer and incubated

overnight at 4°C. After washing with PBST (PBS, 1 mM EDTA, 0.05% Tween-20), the plates were blocked with 5% BSA in PBS for 30 minutes at room temperature. Serum was diluted to the appropriate concentration with blocking buffer and incubated overnight at 4°C. After washing with PBST, the plates were incubated with HRP-conjugated anti-mouse IgG(1033-05; SouthernBiotech) and IgE(1110-05; SouthernBiotech) antibodies (1:2000 in 1% BSA/PBST) at 37°C for 1 hour. Following washing, TMB substrate was added, and the reaction was stopped with 2 M H_2SO_4 after sufficient color development (1–15 minutes). Absorbance at 450 nm was measured within 30 minutes.

Lymphocyte Isolation and Flow Cytometry

Cells from lymphoid organs were prepared by mechanical disruption between frosted slides, while non-lymphoid organs were processed enzymatically. For lung tissue, minced samples were digested in RPMI containing 100 μg/mL DNase I (9003-98-9;Sigma-Aldrich) and 2 mg/mL Collagenase D (LS004188;Worthington Biochemical) at 37°C for 1.5 hours. Liver tissue was minced and digested in RPMI supplemented with 100 μg/mL DNase I and 1 mg/mL Collagenase D at 37°C for 30 minutes, with lymphocytes isolated using a 40-70% Percoll (GE Healthcare) gradient. For intestinal tissue, the samples were first incubated in DMEM containing 3% FBS, 0.2% HEPES, 0.5 M EDTA, and 0.145 mg/mL dithiothreitol for 10 minutes. This was followed by digestion with 50 mg/mL DNase I and 145 mg/mL Collagenase II (Worthington Biochemical) in DMEM at 37°C for 5 minutes. Lymphocytes were then isolated using an 80% and 40% Percoll gradient.

For surface marker analysis, cells were incubated for 15 minutes with purified anti-mouse

CD16/32 antibody (101320; BioLegend) to block Fc receptors. After blocking, cells were stained with the indicated antibodies for surface markers. To determine cytokine expression, cells were stimulated for 4 hours at 37□ with phorbol12-myristate13-acetate (50ng/mL; S1819; Beyotime), ionomycin (1mg/ml; S1672; Beyotime), and brefeldin A (BFA;00-4506-51; Invitrogen). After stimulation, cells were labeled with a fixable viability dye and surface markers. Cells were then fixed and permeabilized according to the manufacturer's instructions (00-8222-49; Invitrogen). For transcription factor staining, samples were fixed using the FOXP3/Transcription Factor Staining Buffer Set (00-5523-00; Invitrogen). Flow cytometry was conducted using a BD Fortessa (BD Biosciences) or LongCyte (Beijing Challen Biotechnology Co., Ltd.) system. Flow cytometry data were acquired and analyzed using FlowJo software.

The following antibodies were purchased from Invitrogen or BioLegend: Zombie Violet f-ixable viability(423113), Zombie NIR fixable(423105), CD25(PC61), CD8α(53-6.7), CD62L(MEL-14), PD-1(J43), CD44(IM7), IL-17A(TC1118H10), KL-RG1(2F1), CD4 (GK1.5), TCRβ(H57-597), IFN-γ(XMG1.2), FOXP3(FJK-16s), CTLA-4(UC10-4B9), ICOS(15F9), GITR(DTA-1), LAG3(C9B7W), TCRVβ11(RR3-15), CD45RB(C363-16A) CD69 (H1.2F3), MHCII(M5/114.15.2), CD80(16-10A1), T-bet(eBio4B10), IKZF4(ESB7C2), IL-4(11B11), CCR7(4B12), CD73(TY/11.8).

Real-time PCR

Total RNA was extracted from T_{reg} cells using the RNAAiso Plus(9109; Takara) reagent according to the manufacturer's instructions, and cDNA synthesis was performed using the

Prime Script RT Reagent Kit (Takara). TB Green Premix Ex Taq (RR420A; Takara) was used for quantitative real-time PCR (qPCR). The expression levels of target mRNA were normalized to the level of *β-actin* expression. The primers for qPCR are as follows:

Cxxc1 qPCR Forward: ATCCGGGAATGGTACTGTCG

Cxxc1 qPCR Reverse: CTGTGGAGAAGATTTGTGGG

β-actin qPCR Forward: CTGTCCCTGTATGCCTCTG

β-actin qPCR Reverse: ATGTCACGCACGATTTCC

$CD4^+T$ and YFP^+ T_{reg} cells adoptive transfer in Experimental autoimmune encephalomyelitis (EAE)

$CD4^+YFP^+$ T_{reg} cells from *Foxp3*^{cre} and *Foxp3*^{cre} *Cxxc1*$^{fl/fl}$ mice were enriched using the Mouse CD4 T Cell Isolation Kit (480005; Biolegend) and then sorted using the BD Aria II flow cytometer. Naïve $CD4^+T$ cells from 2D2 (MOG35-55-specificTCR transgenic) mice were isolated using the Mouse CD4 Naïve T cell Isolation Kit480039 (480039; Biolegend). As previously described[24], 2D2 naïve $CD4^+$ T cells alone (5 x 10^5 per mouse), or 2D2 naïve $CD4^+$ T cells (5x 10^5 per mouse) together with WT or *Foxp3*^{cre}*Cxxc1*$^{fl/fl}$ T_{reg} cells (2x10^5 per mouse), were transferred into *Rag1*$^{-/-}$ mice via the tail vein. One day after cell transfer, the recipient mice were inoculated subcutaneously (s.c.) with 200μg MOG35-55 peptide (MEVGWYRSPFSRVVHLYRNGK; GenemeSynthesis) emulsified in complete Freund's adjuvant (CFA) (F5506; Sigma). Intravenous administration of 200 ng of Pertussis toxin (181; List Biological Laboratories) was performed on days 0 and 2 after peptide inoculation. The severity of EAE was monitored and blindly graded using a clinical score from 0 to 5: 0, no

clinical signs; 1, limp tail; 2, paraparesis (weakness, incomplete paralysis of one or two hind limbs); 3, paraplegia (complete paralysis of two hind limbs); 4, paraplegia with forelimb weakness or paralysis; 5, dying or death.

Isolation lymphocytes from the central nervous system（CNS）

On day 14 after EAE induction, mice were perfused with transcardially administered PBS to eliminate contaminating blood cells in the central nervous system (CNS). The forebrain and cerebellum were dissected to expose the spinal cord, which was then carefully removed from the spinal canal. The fresh spinal cord was harvested and cut into 2 mm pieces. The CNS tissue pieces were homogenized using a syringe and passed through a 70 μM cell strainer to obtain a single-cell suspension. The single-cell suspension was digested with collagenase D (2μg/ml;11088858001; Roche) and deoxyribonuclease I (DNase I; 1 μg/ml; DN25; Sigma-Aldrich) at 37°C for 20 minutes under rotation. After digestion, the cell suspension was centrifuged to pellet the cells. The cell pellets were resuspended in 40% Percoll and layered onto a discontinuous Percoll gradient. Centrifugation at 80% Percoll allowed for the separation of cells at the 40–80% Percoll interface, which were collected as CNS mononuclear cells. The collected CNS mononuclear cells were washed with PBS to remove any remaining Percoll. CNS mononuclear cells were stimulated for 4 hours with PMA and ionomycin in the presence of Brefeldin A to induce cytokine production. After stimulation, cells were fixed, rendered permeable, and stained with appropriate antibodies for intracellular cytokine detection.

Histological analyses

The lungs, skin, liver, and colon were excised from three-week-old mice. Prior to histological analysis, the samples were fixed in formalin, embedded in paraffin, and stained with hematoxylin and eosin. For CNS histology, spinal cords were fixed in 4% paraformaldehyde, paraffin-embedded, sectioned, and stained with Luxol Fast Blue and hematoxylin and eosin (H&E). To examine colon histology, colons from *Rag1*$^{-/-}$ hosts were similarly processed and stained with H&E.

Adoptive transfer colitis model

Colitis was induced following the protocol described[25]. In brief, CD4^{+} YFP^{+} T_{reg} cells were isolated from 3-week-old CD45.2^{+}*Foxp3*^{cre}*Cxxc1*$^{fl/fl}$ and CD45.2^{+} *Foxp3*^{cre} mice. A total of 2x10^{5} T_{reg} cells from each group were mixed with 4x10^{5} T_{eff} cells (CD45.1^{+}CD4^{+}CD45RB^{hi}) sorted from CD45.1^{+} mice and transferred into the *Rag1*$^{-/-}$ mice via intraperitoneal injection. T_{eff} cells alone were transferred as a control group. Mouse body weight was measured weekly post-adoptive transfer. The percentage change in body weight was calculated by comparing the current weight with the initial weight on day 0. Mice were euthanized when any had reached 80% of their initial body weight. The large intestines were sectioned into 4μm thick slices and stained with hematoxylin.

In vitro T_{reg} suppression assay

Naïve CD4^{+} T cells isolated from WT mice were labeled with CFSE (C34554; Invitrogen). CD4^{+}YFP^{+} T_{reg} cells from *Foxp3*^{cre} and *Foxp3*^{cre}*Cxxc1*$^{fl/fl}$ mice were cultured with naïve

$CD4^+$ T cells ($1\square10^5$ cells) at various ratios in the presence of 2μg/mL anti-CD3(16-0031-85; Invitrogen) and 3μg/mL anti-CD28(16-0281-85; Invitrogen). On day 3, cells were analyzed by flow cytometry.

CUT&Tag

CUT&Tag assays of $CD4^+YFP^+$ T_{reg} cells were conducted as previously described[26]. Briefly, approximately $1x10^5$ single cells were carefully pipetted into wash buffer twice. The pelleted cells were resuspended in wash buffer, activated concanavalin (BP531; Bangs Laboratories), and incubated for 15 minutes at room temperature. Cells bound to the beads were resuspended in Dig-Wash Buffer and incubated with a 1:50 dilution of primary antibodies (rabbit anti-H3K4me3, Active Motif,39016; rabbit anti-CXXC1, abcam, ab198977; rabbit anti-FOXP3, abcam, ab 150743;normal IgG, Cell Signaling, 2729) at 4 □ overnight. The beads were incubated with a secondary antibody (goat anti-rabbit IgG; SAB3700883; Sigma-Aldrish) diluted 1:100 in Dig-Wash buffer for 60 minutes at room temperature. Cells were treated with Hyperactive pG-Tn5 Transposase (S602; Vazyme) diluted in Dig-300 Buffer for 1 hour at room temperature. The cells were subsequently resuspended in Tagmentation buffer (10mM MgCl2 in Dig-300 Buffer) and incubated at 37□ for 1 hour. To halt tagmentation, 10μl was spiked with 0.5M EDTA, 3μl with 10%SDS, and 3μl with 20mg/ml Proteinase K and incubated at 55□ for 1h. DNA library amplification was performed according to the manufacturer's instructions and purified using VAHTS DNA Clean Beads (N411; Vazyme). Libraries were sequenced on the Illumina NovaSeq platform (Annoroad Gene Technology).

CUT&Tag and ChIP-seq data analysis

FOXP3 ChIP-seq data was obtained from GSE121279. H3K27me3 ChIP-seq data was obtained from GSE14254. CUT&Tag and ChIP-seq reads were trimmed to 50 bp and aligned against the mouse genome build mm9 using Bowtie2(v2.3.4.1) with default parameters. All PCR duplicates and unmapped reads were removed. Peak calling was performed using MACS2(v2.1.1.20160309) and signal tracks for each sample were generated using the 'wigToBigWig' utility of UCSC. We classified the H3k4me3 peaks around TSSs into three groups: broad (>5 kb), medium (1-5kb), and narrow (<1 kb). The top 5% of the widest peaks were considered as broad peaks. The average intensity profiles were generated using deepTools (v2.5.4). Motif analysis was performed using the 'findmotifsGenome.pl' command inHomer2 package. Epigenetic factors were identified using the Epigenetic Factor Database(https://epifactors.autosome.org/) and then screened for those that exclusively regulate the expression of their target genes by modulating the deposition of H3K4me3. Genomic distribution was analyzed using the "genomation" R package. GO pathway analysis was performed using the "clusterProfiler" R package. The sequencing information of CUT&Tag data used in this study is summarized in Supplementary Table S1.

Clustering analysis

Promoters were defined as ±2 kb regions flanking the annotated TSS. Reads in promoters were counted using the "coverage" command in bedtools (v2.26.0) and further normalized to RPKM. The k-means clustering of H3K4me3 and H3K27me3 enrichment at promoters was conducted using the "kmeans" function in R.

RNA-seq and data analysis

Total RNA was extracted from sorted CD4□YFP□ T_{reg} cells using the RNeasy Plus Mini Kit (Qiagen, #74134), following the manufacturer's protocol. RNA-Seq libraries were constructed and sequenced by Haplox (Nanchang, China), using an Illumina platform with paired-end reads of 150 bp. RNA-seq data was obtained from GSE82076. Raw reads were trimmed to 50 bp and mapped to the mouse genome (mm9) using TopHat (v2.1.1) with default parameters. Only uniquely mapped reads were kept for downstream analysis. The RNA abundance of each gene was quantified using Cufflinks (v2.2.1).

Single-Cell RNA-Sequencing

A total of 300,000 sort-purified $CD4^{+}YFP^{+}$ T_{reg} cells from *Foxp3*^{cre} and *Foxp3*^{cre} *Cxxc1*$^{fl/fl}$ were resuspended in BD Pharmingen Stain Buffer (FBS) (554656; BD). Single cells were isolated using a chromium controller (BD platform, BD Bioscience) according to the manufacturer's instructions, as previously described[27]. The single cells were labeled with sample tags using the BD Mouse Immune Single-Cell Multiplexing Kit (633793; BD). Following standard protocols, cDNA amplification and library construction were performed to generate scRNA-seq libraries.

Targeted scRNA-seq data processing

The raw FASTQ files were processed by BD Rhapsody using the Targeted analysis pipeline. After alignment and filtering, the distribution-based error correction(DBEC)-adjusted molecules were loaded into R studio(version 4.3.2). All subsequent analyses were performed

using the package Seurat (version 4.4.0) with default parameters. Specifically, the scRNA-seq data counts were log-normalized. All targeted genes were scaled and then were used for Principal components analysis (PCA). The batch effects were removed by the HarmonyMatrix function in the Harmony package (version 1.1.0). The first 20 principal components were used to calculate nonlinear dimensionality reduction using RunUMAP. Differential gene expression (DEGs) between clusters was assessed using the FindAllMarkers function. The clusters were then annotated based on DEGs. Barplots were generated using ggplot2 (version 3.4.4). Heatmaps were generated using pheatmap (version 1.0.12).

Analysis of the single-cell TCR-seq repertoire

Raw V(D)J fastq reads were processed using BD Rhapsody Pipeline and then were analyzed using scRepertoire (version 1.12.0). The TCR clonotype was called using the nucleotide sequence of the CDR3 region for both TCR alpha and beta chains. For cells with multiple chains, the top two clonotypes with the highest expression were selected for downstream analysis. Clonal overlap between different cell types was calculated using the clonalOverlap function of scRepertoire. A clonotype was defined as expansion if it could be detected in at least two cells.

scRNA-seq trajectory analysis

UMAP embeddings obtained from the Seurat package were projected into the Slingshot(version 2.10.0) package to construct pseudotime Trajectories for T_{reg} cells. Naïve subsets were set as the root state.

Whole genome bisulfite sequencing (WGBS) and data analysis

Sorted $CD4^{+}YFP^{+}$ T_{reg} cells(3×10^{6}) were lysed in cell lysis buffer to release DNA. The bisulfite-treated DNA was used to prepare the sequencing library. DNA libraries were transferred to the Illumina Platform for sequencing using 150 bp paired-end reads. Raw reads were trimmed using TrimGalore (v0.4.4) with default parameters. Subsequently, the reads were mapped against the mm9 reference genome using Bismark v0.19.0 with parameters '--bowtie2'. PCR duplicates were removed and the methylation levels were calculated using 'bismark_methylation_extractor'. We calculated the mean CpG methylation levels of various genome elements: promoter, 5′-UTR, exon, intron, 3′-UTR, genebody, intergenic, CGIs, and repeats using in-house scripts. The sequencing information of WGBS data used in this study is summarized in Supplementary Table S2.

Statistical analysis

The statistical significance analysis was performed using Prism 8.0 (GraphPad). Error bars are presented as mean ± SD. P values of < 0.05 were deemed statistically significant (*$P < 0.05$, **$P < 0.01$, ***$P < 0.001$ and ****$P < 0.000$). Statistical analyses were performed with unpaired Student's *t*-test or two-way ANOVA and Holm–Sidak post hoc test.

Results

FOXP3 binds regulatory loci primed for activation and repression in T_{reg} cells

FOXP3-mediated gene expression is well-recognized, with several studies highlighting its

348 dual role as both a transcriptional activator and repressor [28-32]. However, the mechanisms by
349 which FOXP3 regulates T_{reg}-specific gene transcription via epigenetic modifications remain
350 incompletely understood. To investigate these mechanisms, we employed CUT&Tag to
351 generate genome-wide H3K4me3 maps in T_{reg} cells. To complement this, we compared our
352 data with an H3K27me3 ChIP-Seq dataset from Wei *et al.*[33] focusing on previously identified
353 FOXP3-bound loci(Konopacki *et al*. 2019)[34]. This integrative analysis allowed us to identify
354 FOXP3-dependent genes associated with either H3K4me3 (indicative of transcriptional
355 activation) or H3K27me3 (indicative of repression) deposition. These findings provide
356 insight into how FOXP3 modulates the epigenetic landscape to regulate T_{reg} cell function.
357 As expected, H3K4me3 was enriched at gene promoters (fig. S1, A and B). A Venn diagram
358 revealed overlap between FOXP3 binding sites and H3K4me3 peaks, with minimal overlap
359 with H3K27me3 peaks (Fig. 1, A and B). The overlapping regions between FOXP3 binding
360 sites and H3K4me3 or H3K27me3 peaks were predominantly located at promoters (Fig. 1, A
361 and B). To further investigate the role of FOXP3 in promoting H3K4me3 deposition, we
362 compared H3K4me3 levels between FOXP3-positive T_{reg} cells and FOXP3-negative
363 conventional T cells (Tconv). Consistent with our hypothesis, H3K4me3 abundance was
364 higher at T_{reg}-specific gene loci (e.g., *Tnfrsf18*, *Ctla4*, *Il2ra* and *Nt5e*) in T_{reg} cells compared
365 to Tconv cells (Fig. 1,C and fig. S1, C). Notably, the selection of these loci was guided by
366 prior studies identifying genes specifically associated with T_{reg} cell function[35]. This finding
367 highlights the role of FOXP3 in shaping the epigenetic landscape of T_{reg} cells through
368 enhanced H3K4me3 deposition at these critical loci.
369 To further characterize these modifications,we clustered promoters into four groups based on

the enrichment of H3K4me3 and H3K27me3. Clusters 1 and 3 showed strong enrichment of H3K4me3; cluster 2 was enriched with H3K27me3; and cluster 4 showed weak enrichment of both modifications. FOXP3 preferentially bound to clusters 1 and 3 prom-oters, which displayed high H3K4me3 levels (Fig. 1C). Correspondingly, genes in these clusters exhibited high transcription levels, as shown by reanalysis of previously published RNA-seq data (Oh *et al.* 2017) [36] (Figure 1D, right) . In contrast, genes with H3K27me3 enrichment at their promoters were transcribed at low levels.

Gene Ontology (GO) analysis of these four clusters revealed distinct functional roles. Cluster 1 was enriched in genes involved in mRNA processing, covalent chromatin modification, and histone modification, while cluster 3 was enriched in genes related to DNA repair and mitochondrion organization (Fig. 1E). Cluster 2, enriched with H3K27me3, was associated with pattern specification process, while cluster 4 showed no correlation with T_{reg} cells. Notably, signature T_{reg} cell genes such as *Tnfrsf18*, *Nrp1*, *Stat5a*, *Lag3*, *Icos*, and *Pdcd1* were enriched in clusters 1 and 3, showing strong H3K4me3 marks (fig. S1C). Conversely, genes like *Hic1*, *Trp73*, and *Rnf157*, associated with inflammatory responses, were enriched for H3K27me3 in clusters 2 (fig. S1C). These findings collectively support the conclusion that FOXP3 contributes to transcriptional activation in T_{reg} cells by promoting H3K4me3 deposition at target loci, while also regulating gene expression directly or indirectly through other epigenetic modifications.

CXXC1 interacts with FOXP3 and binds H3K4me3-enriched sites in T_{reg} cells

We conducted an enrichment analysis of known motifs at the overlapping peaks of FOXP3

ChIP-seq and H3K4me3 CUT&Tag in T_{reg} cells to identify epigenetic factors that directly interact with FOXP3 to mediate chromatin remodeling and transcriptional reprogramming. Motif analysis of the overlapping peaks between FOXP3 binding sites and regions enriched in H3K4me3 revealed that, in addition to transcription factors, the most abundant motif associated with H3K4me3 was the epigenetic factor CXXC1(fig. S2A). To investigate this further, we performed CUT&Tag for endogenous CXXC1 in T_{reg} cells to examine the genome-wide co-occupancy of CXXC1 and FOXP3. Over half of these CXXC1 binding sites were located at promoter regions (fig. S2B). Additionally, CXXC1 exhibited strong binding at transcription start site (TSS) and CpG islands (CGIs)(Fig. 2A and fig. S2C). As illustrated by the Venn diagram (Fig. 2B), more than half of the FOXP3-bound genes and H3K4me3-enriched genes were also bound by CXXC1. Similarly, more than half of CXXC1 peaks were overlapped with FOXP3 peaks (fig. S2D). Furthermore, the CXXC1-specific and FOXP3-specific binding sites also demonstrated modest binding of FOXP3 and CXXC1, respectively (Fig. 2C). These findings indicate that FOXP3 and CXXC1 share a substantial number of target genes in T_{reg} cells. To confirm this interaction, we further validated the reciprocal immunoprecipitation of both endogenous and exogenous CXXC1 and FOXP3 (Fig. 2D and fig. S2E). An immunofluorescence assay revealed predominant colocalization of CXXC1 with FOXP3 in the nucleus (Fig. 2E). Overall, these results suggest that CXXC1 primarily functions as a coactivator of FOXP3-driven transcription in T_{reg} cells.

Complete ablation of *Cxxc1* in T_{reg} cells leads to a fatal autoimmune disease

To investigate the role of CXXC1 in T_{reg}-cell homeostasis and function, we generated *Foxp3*^{Cre}*Cxxc1*$^{fl/fl}$ mice (conditional knockout [cKO] mice) by crossing *Cxxc1*$^{fl/fl}$ with *Foxp3*$^{YFP\text{-}Cre}$ [37] mice, thereby specifically deleting *Cxxc1* in T_{reg} cells. The effective depletion of *Cxxc1* in T_{reg} cells was confirmed through quantitative PCR (qPCR) and Western blotting (fig. S3A). Notably, cKO mice appeared normal at birth but later exhibited spontaneous mortality starting around three weeks of age (Fig. 3A). Deletion of *Cxxc1* in T_{reg} cells led to the development of severe inflammatory disease, characterized by reduced body size, stooped posture, crusting of the eyelids, ears, and tail, and skin ulceration, particularly on the head and upper back (Fig. 3, B and C). Additionally, cKO mice developed extensive splenomegaly and lymphadenopathy (Fig. 3D). *Foxp3*^{Cre}*Cxxc1*$^{fl/fl}$ mice exhibited elevated serum levels of anti-dsDNA autoantibodies and IgG , along with a modest increase in IgE concentration (Figure 3E and fig. S3B). Histopathological analysis revealed massive lymphocyte and myeloid cell infiltration in the skin, lungs, liver sinusoids, and colon mucosa (Fig. 3F). In full agreement with the aforementioned severe autoimmune diseases, *Foxp3*^{Cre}*Cxxc1*$^{fl/fl}$ mice had decreased percentages and numbers of CD4^{+} Foxp3^{+} T_{reg} cells in small intestine lamina propria (LPL), liver and lung(Fig. 3G and fig. S3C). Moreover, cKO mice displayed an increase in CD8^{+} T cell percentages (fig. S3D), along with a marked rise in cells exhibiting an effector/memory phenotype (CD44hi CD62Llo) (Fig. 3H). Furthermore, T cells from cKO mice produced elevated levels of IFN-γ, IL-17, and IL-4 in CD4^{+} YFP^{-} T cells, as well as increased IFN-γ production in CD8^{+} T cells (Fig. 3I and fig. S3, E and F). These phenotypes closely resembled those observed in *Foxp3*-deficient mice [38] or mice with depleted T_{reg} cells[39],

suggesting a deficiency in immune suppression.

CXXC1 is necessary for the maintenance of T_{reg}-cell suppressive activity

Despite the development of severe autoimmune disease, we observed an increase in both the absolute number and percentage of FOXP3^{+} T_{reg} cells in the lymph nodes (fig. S4A). The expression level of the FOXP3 protein was only slightly altered in *Cxxc1*-deficient T_{reg} cells (fig. S4B). In an *in vitro* suppression assay, T_{reg} cells from *Foxp3*^{Cre}*Cxxc1*$^{fl/fl}$ and WT mice exhibited similar suppressive effects on naïve T (Tn) cell proliferation (fig. S4C). The expression of the hallmark T_{reg}-cell marker CTLA-4 showed a modest increase in *Cxxc1*-deficient T_{reg} cells compared to WT T_{reg} cells, while the expression of GITR remained unchanged (fig. S4D). To further assess the suppressive capacity of *Cxxc1*-deficient T_{reg} cells *in vivo*, we employed the experimental autoimmune encephalomyelitis (EAE) model. Naïve CD4^{+} T cells from 2D2 mice were co-transferred with T_{reg} cells from either *Foxp3*^{Cre} or *Foxp3*^{Cre} *Cxxc1*$^{fl/fl}$ mice into *Rag1*$^{-/-}$ recipients, and EAE was induced in these recipient mice. Mice that received only naïve CD4^{+} T cells from 2D2 mice developed more severe EAE symptoms (Fig. 4A). The addition of WT T_{reg} cells from *Foxp3*^{Cre} mice slightly mitigated EAE progression and reduced Th17 cells in the spinal cord (Fig. 4, A to D). In contrast, *Foxp3*^{Cre} *Cxxc1*$^{fl/fl}$ T_{reg} cells failed to suppress EAE (Fig. 4, A to D), and the cKO mice showed a reduction in T_{reg} cells frequency in CNS tissues(Fig. 4E). Finally, we examined the role of CXXC1 in T_{reg} cell-mediated suppression using T cell transfer-induced colitis, in which naïve T cells were transferred to *Rag1*$^{-/-}$ recipients either alone or together with WT or *Foxp3*^{Cre} *Cxxc1*$^{fl/fl}$ T_{reg} cells. The transfer of naïve T cells led to weight loss and intestinal

pathology in recipient mice(Fig. 4, F and G). Mice receiving WT T_{reg} cells continued to gain weight (Fig. 4F) , whereas those that received T_{reg} cells from cKO mice were unable to prevent colitis and exhibited a reduced percentage of T_{reg} cells (Fig. 4, F to H). These findings underscore the critical role of CXXC1 in maintaining T_{reg} cell function *in vivo*.

T_{reg} cell lineage homeostasis and proliferation depend upon CXXC1

T_{reg} cells harbor a diverse T-cell receptor (TCR) repertoire, which likely play a critical role in their immune suppression function [40-42]. To explore the role of CXXC1 in T_{reg}-mediated suppression, we performed single-cell RNA sequencing (scRNA-seq) combined with TCR sequencing (TCR-seq) on $CD4^+YFP^+$ T_{reg} cells isolated from mouse lymph nodes. After quality control and removal of doublets, 18,577 cells were retained for further analysis. Through unsupervised clustering and uniform manifold approximation and projection (UMAP) analysis, we identified eight distinct T_{reg} cell clusters based on the expression of well-characterized markers, with a particular focus on two clusters of activated T_{reg} cells that exhibited higher expression of markers and gene sets relative to naïve T_{reg} cells (Fig. 5A and fig. S5, A to C). A comparison between *Cxxc1*-deficient and WT T_{reg} cells within each cluster revealed a reduction in *Cxxc1*-deficient cells in the naïve subsets, while an increase was observed in the $Gzmb^+$ and $H2\text{-}Eb1^+$ subsets (Fig. 5B). To further elucidate the transition of T_{reg} cells along a dynamic biological timeline, we constructed pseudo-time trajectories using Slingshot [43]. The pseudo-time gradient depicted a progression from quiescent to activated T_{reg} cells, ultimately encompassing the $Gzmb^+$ and $H2\text{-}Eb1^+$ subsets (Fig. 5C). Given the antigen-specific suppression capabilities of T_{reg} cells [44,45], we examined their clonal

expansion. The analysis revealed that expanded WT TCR clonotypes (n≥2) were predominantly distributed among the Nt5e^{+} subsets, while *Cxxc1*-deficient T_{reg} cells showed expanded clonotypes primarily within the Gzmb^{+} and H2-Eb1^{+} subsets(Fig. 5D and Fig. S5D). TCR sharing analysis indicated clonotype sharing among various clusters of WT T_{reg} cells, suggesting a degree of homogeneity. However, the reduced TCR sharing in *Cxxc1*-deficient T_{reg} cells implies that decreased TCR diversity may impair the suppressive activity of T_{reg} cells (Fig. 5E) [42]. Furthermore, the *Cxxc1*-deficient group exhibited lower expression of several T_{reg}-specific genes associated with suppressive functions, such as*Nt5e*, *Il10*, *Pdcd1*, *Klrg1*, as well as genes that inhibit effector T cells differentiation, including *Sell* and *Tcf7* (Fig. 5F and fig. S5E). Conversely, *Cxxc1*-deficient T_{reg} cells demonstrated elevated expression of *Gzmb*, *Il2ra*, and *Cd69* compared to WT, reflecting a profile indicative of increased activation (Fig. 5, F and G). Additionally, we observed increased expression of genes linked to Th1-type inflammation, such as *Ifng*, *Tbx21*, and *Hif1a*, in *Cxxc1*-deficient T_{reg} cells, likely due to extreme inflammatory conditions (Fig. 5, F to H). The proportion of FOXP3^{+}Ki67^{+} T_{reg} cells was lower in cKO mice compared to WT mice (Fig. 5I). These findings underscore the crucial role of CXXC1 in in maintaining T_{reg} cell function and homeostasis.

Intrinsic *Cxxc1* deficiency impairs T_{reg} cell suppression, proliferation, and molecular programs.

To confirm that the deficiency in T_{reg} cell function in T_{reg}-specific *Cxxc1*-deficient animals is due to intrinsic defects caused by *Cxxc1* deficiency, rather than severe autoimmune

inflammation in *Foxp3*^{Cre} *Cxxc1*$^{fl/fl}$ mice, we examined *Cxxc1*-sufficient and *Cxxc1*-deficient T_{reg} cell subsets in heterozygous *Foxp3*$^{Cre/+}$ *Cxxc1*$^{fl/fl}$ (designated as "het-KO") and littermate *Foxp3*$^{Cre/+}$ *Cxxc1*$^{fl/+}$ (designated as "het-WT") female mice (Fig. 6A). Notably, het-KO female mice did not exhibit overt signs of autoimmunity, as random X-chromosome inactivation led to the coexistence of both *Cxxc1*-cKO and *Cxxc1*-WT T_{reg} cells. However, both the frequency and absolute numbers of FOXP3^{+}YFP^{+} T_{reg} cells within the total T_{reg} population were reduced in het-KO mice compared to their counterparts in het-WT littermates, indicating that *Cxxc1* deficiency imposes a competitive disadvantage on T_{reg} cells (Fig. 6B). Additionally, *Cxxc1*-deficient YFP^{+} T_{reg} cells failed to upregulate the proliferation marker Ki-67 (Fig. 6C). Moreover, YFP^{+} T_{reg} cells in het-KO female mice showed reduced expression of key genes essential for suppressive function, including ICOS, CD25,CTLA4, and GITR, compared to YFP^{-}T_{reg} cells from the same mice (Fig. 6D). Consistently, we confirmed the impaired suppressive function of T_{reg} cells from heterozygous *Foxp3*$^{Cre/+}$ *Cxxc1*$^{fl/fl}$ mice in *vitro* and in *vivo* (Fig. 6E and fig. S6A-E). To investigate the molecular program affected by the deletion of *Cxxc1* in T_{reg} cells, we performed RNA-sequencing (RNA-seq) analysis on CD4^{+}YFP^{+} T_{reg} cells isolated from het-WT and het-KO mice. We then conducted a differential gene expression (DGE) analysis based on the RNA-seq data. Among all expressed genes, 865 were upregulated ("Up" genes) and 761 were downregulated ("Down" genes) by ≥1.5-fold in CD4^{+}YFP^{+} T_{reg} cells from het-KO mice compared to het-WT mice, with a false discovery rate (FDR)–adjusted *P*-value cutoff of 0.05 (fig. S6F). Gene Ontology (GO) enrichment analysis revealed that the downregulated genes in *Cxxc1*-deficient T_{reg} cells were predominantly enriched in pathways related to the negative regulation of immune system

process and regulation of cell−cell adhesion (fig. S6G). The *Cxxc1*-deficient T_{reg} cells also showed reduced expression of several genes associated with T_{reg} cell suppressive function, including *Il10*, *Tigit*, *Lag3*, *Icos*, *Nt5e*(encoding CD73) and *Itgae* (encoding CD103) (fig. S6H). Thus, while YFP□ WT T_{reg} cells effectively prevent autoimmunity in het-KO mice, the absence of *Cxxc1* in YFP□ T_{reg} cells disrupts key T_{reg} cell marker expression and impairs their suppressive function under steady-state conditions.

The FOXP3-CXXC1 complex regulates the expression of key factors in T_{reg} cells that are associated with the breadth of H3K4me3

CXXC1 binds to unmethylated CpG DNA via its N-terminal CXXC finger domain, facilitating its interaction with DNA methyltransferase 1 (DNMT1). This binding stabilizes the DNMT1 protein, thereby regulating DNA methylation [46,47]. To investigate whether CXXC1 depletion affects DNA methylation in T_{reg} cells, we performed whole genome bisulfite sequencing (WGBS) on T_{reg} cells isolated from both WT and cKO mice. On average, *Cxxc1*-deficient T_{reg} cells exhibited no changes in DNA methylation at gene loci or across genome-wide CpG sites, irrespective of chromosomal region (fig. S7, A to C). Furthermore, *Cxxc1* knockout T_{reg} cells did not show a increase in DNA methylation at key T_{reg} signature gene loci (fig. S7D). Given the pivotal role of MLL4-mediated H3K4me1 in establishing the enhancer landscape and facilitating long-range chromatin interactions during T_{reg} cell development[15], we performed CUT&Tag to assess changes in H3K4me1 levels in *Cxxc1*-deficient T_{reg} cells. This analysis revealed that H3K4me1 levels were similar in both WT and *Cxxc1*-deficient T_{reg} cells (fig. S7, E to G).

While H3K4me3 modifications typically form sharp 1-to 2-kb peaks around promoters, some genes exhibit broader H3K4me3 regions, referred to as broad H3K4me3 domains (H3K4me3-BDs), which can extend to cover part or all of the gene's coding sequences (up to 20 kb) [48,49]. Broad H3K4me3 domains are preferentially associated with genes essential for the identity or function of specific cell types [48,50] and have been implicated in enhancing transcriptional elongation and increasing enhancer activity [50]. To further explore the connection between broad H3K4me3 domains and the expression of immune-regulatory genes, we analyzed genes containing broad H3K4me3 regions. We classified the H3K4me3 domains surrounding transcription start sites (TSSs) into three categories: broad (more than 5 kb), medium (between 1 and 5 kb), and narrow (less than 1 kb) (Fig. 7A). Notably, *Cxxc1*-deficient T_{reg} cells exhibited weaker H3K4me3 signals compared to WT cells within the broad H3K4me3 domains where CXXC1 binding is prominent (Fig. 7, A and B). Using the criteria established by Benayoun *et al.*[48], which defines the top 5% of the widest H3K4me3 domains as BDs, we observed similar enrichment results (fig. S7, H and I). We then compared three groups of genes: BD-associated genes with reduced H3K4me3 levels following *Cxxc1* deletion, genes with direct CXXC1 binding, and genes with direct FOXP3 binding. The Venn diagram revealed that the majority of genes (283 out of 294, 96%) with CXXC1 binding and reduced H3K4me3 levels overlap with FOXP3-bound genes, suggesting that CXXC1 presence enhances FOXP3 binding within the broad H3K4me3 domain (Fig. 7C). Furthermore, GO term analysis indicated that BD-associated genes are enriched in biological processes related to the negative regulation of immune system processes (Fig. 7D). Genome browser views displayed the enrichments of FOXP3, CXXC1, and H3K4me3 at key

signature genes in T_{reg} cells, such as *Ctla4*, *Il2ra*, *Icos*, and *Tnfrsf18*, with lower H3K4me3 densities observed at these loci in *Cxxc1*-deficient T_{reg} cells (Fig. 7E). Similar patterns were observed at core genes involved in T_{reg} homeostasis and suppressive function (e.g., *Lag3*, *Nt5e*, *Ikzf4*, and *Cd28*) (fig. S7, J)[51,52]. These findings suggest that CXXC1 and FOXP3 collaboratively promote sustained T_{reg} cell homeostasis and function by preserving the H3K4me3 modification at key T_{reg} cell genes.

We previously demonstrated that the FOXP3-CXXC1 complex plays a key role in modulating H3K4me3 deposition at T_{reg}-specific gene loci. To further clarify whether *Cxxc1* deletion affects FOXP3 binding to its target genes, we performed CUT&Tag experiments to compare FOXP3 binding profiles between WT and *Cxxc1* KO T_{reg} cells. The results revealed that most FOXP3-bound regions in WT T_{reg} cells were similarly enriched in KO T_{reg} cells, indicating that *Cxxc1* deletion does not impair FOXP3's DNA-binding ability (fig. S8A and B). Together, these findings suggest that the regulatory role of CXXC1 in T_{reg} cells is mediated through its effect on H3K4me3 deposition rather than altering FOXP3's binding to DNA.

Discussion

T_{reg} cells specifically express the transcription factor FOXP3, which is essential for maintaining T_{reg} lineage stability and suppressive function[53]. However, FOXP3 alone is insufficient to fully regulate the transcriptional signature and functionality of T_{reg} cells; its interaction with protein partners is crucial for this regulation. In this study, we identify CXXC1 as a critical epigenetic regulator and functional cofactor of FOXP3. Although

582 CXXC1 is not required for FOXP3's DNA-binding activity, as evidenced by similar FOXP3
583 binding patterns in WT and *Cxxc1*-deficient T_{reg} cells (CUT&Tag analysis), it plays an
584 essential role in maintaining H3K4me3 modifications at FOXP3 target loci. By acting as both
585 an epigenetic regulator and a FOXP3 cofactor, CXXC1 ensures the stability of the T_{reg}
586 transcriptional program, highlighting its pivotal role in preserving T_{reg} cell functionality and
587 immune homeostasis.

588 FOXP3 is known to promote histone H3 acetylation at the promoters and enhancers of its
589 target genes, such as *Il2ra*, *Ctla4*, and *Tnfrsf18*, following T_{reg} cell activation, thereby
590 functioning as a transcriptional activator[54,55]. Conversely, FOXP3 can act as a repressor by
591 silencing target genes like *Il2* and *Ifng* through the induction of histone H3 deacetylation,
592 mediated by the recruitment of histone deacetylases and transcriptional co-repressors[10,56].
593 Additionally, FOXP3 exerts this repression by recruiting the Ezh2-containing polycomb
594 repressive complex to target genes during activation, as FOXP3-repressed genes are
595 associated with H3K27me3 deposition and reduced chromatin accessibility[11,57]. Recent
596 studies have begun to explore the biological significance of H3K4me3 breadth, revealing a
597 positive correlation between H3K4me3 breadth and gene expression [50,58,59]. These studies
598 also suggest that H3K4me3 breadth contributes to defining specific cell identities during
599 development and disease, including systemic autoimmune diseases like systemic lupus
600 erythematosus and various cancers [48,60-63]. Our study demonstrates that the loss of *Cxxc1*
601 leads to reduced H3K4me3 levels, predominantly in genes with broader peaks, such as *Il2ra*,
602 *Tnfrsf18, Ctla4 and Icos*, directly impairing their suppressive function in T_{reg} cells. Although
603 our research primarily focused on the role of CXXC1 in T_{reg} cells, it is plausible that similar

mechanisms may be operative in other cell types.

The T_{reg}-specific deletion of *Cxxc1* leads to a rapid and fatal autoimmune disorder, characterized by systemic inflammation and tissue damage, underscoring the essential role of CXXC1 in maintaining immune self-tolerance within T_{reg} cells. Interestingly, despite this severe phenotype, our findings show that H3K4me1 levels were comparable between WT and *Cxxc1*-deficient T_{reg} cells. In contrast, MLL4 is critical for T_{reg} cell development in the thymus, primarily by regulating H3K4me1, though it is not required for peripheral T_{reg} cell function[15]. Numerous studies investigating the effectors of T_{reg} cell-mediated suppression have identified a wide range of molecules and mechanisms. These include the upregulation of the inhibitory co-stimulatory receptor CTLA-4, which initiates inhibitory signaling; the sequestration of the T-cell growth factor IL-2 via CD25; the secretion of inhibitory cytokines, such as interleukin (IL)-10, IL-35 and TGF-β and the activity of ectoenzymes CD39 and CD73 on the T_{reg} cells surface, which convert extracellular ATP, a potent pro-inflammatory mediator, into its anti-inflammatory counterpart, adenosine[42,64]. Mechanistically, we demonstrated that CXXC1 interacts with FOXP3 to regulate T_{reg} cell function by trimethylating H3K4 at broad H3K4me3 domains of multiple genes involved in suppressive functions such as *Il2ra*, *Nt5e, and Ctla4*. Additionally, MLL1, another KMT, controls T_{reg} cell activation and function by specifically regulating H3K4 trimethylation at genes encoding key T_{reg}-related molecules such as *Tigit*, *Klrg1*, *Tbx21*, *Cxcr3*, and serves as a crucial epigenetic regulator in establishing a stable Th1-T_{reg} lineage[14].

Our findings demonstrate that *Cxxc1*-deficient T_{reg} cells exhibit reduced H3K4me3 levels at T_{reg}-specific loci, indicating that CXXC1 plays a critical role in regulating this epigenetic

modification. This is consistent with previous studies showing that CXXC1 acts as a non-catalytic component of the Set1/COMPASS complex [65-68], which includes the H3K4 methyltransferases SETD1A and SETD1B, the primary enzymes responsible for H3K4 trimethylation. Given this, we propose that CXXC1 supports H3K4me3 deposition in T_{reg} cells by interacting with and stabilizing the activity of the Set1/COMPASS complex. Further studies are required to directly investigate the interactions between CXXC1 and these methyltransferases in the T_{reg} cell context.

Our results offer provide novel insights into the suppressive functions, heterogeneity, and regulatory mechanisms of T_{reg} cells. Maintaining T_{reg} cell homeostasis and function remains a challenge in harnessing T_{reg} cells for the treatment of autoimmune diseases and the prevention of graft rejection.

Competing interests

The authors declare that they have no competing interests.

Acknowledgments

We thank B. Li (Shanghai Jiao Tong University School of Medicine, Shanghai, China) for providing *Foxp3*$^{YFP\text{-}Cre}$ mice, X.Y. Zhou(Chinese Academy of Science (CAS), Beijing, China) for providing the FOXP3 CUT&Tag antibody, and X. L. Liu (Shanghai Institutes for Biological Sciences, Chinese Academy of Sciences) for his generous gifts of cell lines. We thank Y. Huang, Y. Li, J. Wan, C.Guo, and Z. Lin from the Core Facilities, Zhejiang

University School of Medicine for their technical support and S. Hong, Y. Ding, H. Jin, Q. Wang, and X. Zhang from Animal Facilities, Zhejiang University, for feeding the mice.

Footnotes

This work was supported by grants from the National Natural Science Foundation of China (32341002, 32030035, 32321002, 32100693, and 32270839), the National Key R & D Program of China (2023YFA1800202, 2024YFF0728703, 2022YFA1103702, 2022YFA1103200), the Zhejiang Provincial Natural Science Foundation of China (LZ21C080001, LZ23C070003), Science and Technology Innovation 2030-Major Project (2021ZD0200405), Key project of the Experimental Technology Program of Zhejiang University (SZD202203), and the Fundamental Research Funds for the Central Universities (226-2024-00161).

Author contributions

L.W. and L.S.: supervision, conceptualization, project administration, and writing—review and editing. L.W., L.S. and X.M: funding acquisition. X.M: investigation, methodology, project administration, and writing— original draft. Y.Z.and K.L.: bioinformatics analysis. Y. W., X.L., J.C., C.L., Y.Z., S.W., S.T., Q.X., L.D., X.S., and X.G.: investigation and methodology.

Figure legends

Fig. 1. H3K4me3 is required for FOXP3-dependent gene activation in T_{reg} cells.

(**A**)Venn diagram showing overlap of H3K4me3 enriched regions (this study) and FOXP3 binding sites (Konopacki *et al*.2019) in sorted $CD4^{+}YFP^{+}$ T_{reg} cells (left). Genomic distribution of overlapped peaks(right). Note that the overlapped peaks are predominantly enriched at promoters.

(**B**)Venn diagram showing overlap of H3K27me3 enriched regions (Wei *et al*.2009) and FOXP3 binding sites in T_{reg} cells (left). Genomic distribution of overlapped peaks (right). Note that the overlapped peaks are predominantly enriched at promoters.

(**C**)Representative genome browser view showing the enrichments of H3K4me3 and FOXP3 inTconv or T_{reg} cells.

(**D**)Heatmap showing enrichment of H3K27me3, H3K4me3, and FOXP3 surrounding the TSS. Unsupervised K-means clustering was conducted on H3K27me3 and H3K4me3 signals.

(**E**)Heatmap showing gene expression levels in T_{reg} cells (RNA-seq data was obtained from Oh *et al.*2017) The clusters were consistent as in Fig. 1C.

(**E**)Gene Ontology (GO) pathway analysis of different clusters.

Fig. 2. CXXC1 interacts with FOXP3 in T_{reg} cell.

(**A**)Average CXXC1 CUT&Tag signals around promoters in T_{reg} cells. IgG was used as the control.

(**B**)Venn diagrams showing the overlap of FOXP3 binding genes, CXXC1 binding genes, and H3K4me3 enriched genes in T_{reg} cells. Gene promoters covered by FOXP3 binding sites, CXXC1 binding sites, or exhibited high H3K4me3 levels were defined as FOXP3-bound genes, CXXC1-bound genes, or H3K4me3-enriched genes.

(**C**)Heatmaps showing FOXP3 ChIP-seq and CXXC1 CUT&Tag signals at indicated regions.

(**D**)Interaction between FOXP3 and CXXC1 was assessed by co-IP (forward and reverse) using T_{reg} cell lysates.

(**E**)Immunofluorescence for FOXP3 and CXXC1 colocalization in T_{reg} cells. Scale bars, 2 μm.

Fig.3. *Foxp3*^{cre}*Cxxc1*$^{fl/fl}$ mice spontaneously develop a fatal early-onset inflammatory disorder.

(**A**)Survival curves of *Foxp3*^{cre} (black line) and *Foxp3*^{cre}*Cxxc1*$^{fl/fl}$ (red line) mice (n = 20).

(**B**)Gross body weight of *Foxp3*^{cre} and *Foxp3*^{cre}*Cxxc1*$^{fl/fl}$ mice (n = 6).

(**C**)A representative image of *Foxp3*^{cre} and *Foxp3*^{cre}*Cxxc1*$^{fl/fl}$ mice.

(**D**)Representative images showing the spleen and peripheral lymph nodes from *Foxp3*^{cre} and *Foxp3*^{cre}*Cxxc1*$^{fl/fl}$ mice.

(**E**)ELISA quantification of anti-dsDNA IgG in the serum of *Foxp3*^{cre} and *Foxp3*^{cre}*Cxxc1*$^{fl/fl}$ mice (n = 4).

(**F**)Hematoxylin and eosin staining of the skin, lung, liver, and colon from *Foxp3*^{cre} and *Foxp3*^{cre}*Cxxc1*$^{fl/fl}$ mice (scale bar, 100 μm).

(**G**)Representative flow cytometry plots of CD4 Foxp3 T_{reg} cells isolated from the small intestinal lamina propria (LPL), liver, and lung of *Foxp3*^{cre} and *Foxp3*^{cre}*Cxxc1*$^{fl/fl}$ mice.

(**H**)Flow cytometry analysis of CD62L and CD44 expression on peripheral lymph node $CD4^{+}YFP^{-}$ and $CD8^{+}$T cells from *Foxp3*^{cre} and *Foxp3*^{cre}*Cxxc1*$^{fl/fl}$ mice (left). Right, frequency of $CD44^{low}CD62L^{hi}$ and $CD44^{hi}CD62L^{low}$ population in $CD4^{+}$ YFP^{-} or $CD8^{+}$ T cells (n = 6).

(**I**)Lymph node cells from *Foxp3*^{cre} and *Foxp3*^{cre}*Cxxc1*$^{fl/fl}$ mice were stimulated ex vivo with PMA + ionomycin for 4h and analyzed for IFN-γ expressing in CD4^{+} YFP^{-} or CD8^{+} T cells using flow cytometry (left). Right, percentages of IFN-γ^{+}CD4^{+} YFP^{-} or IFN-γ^{+}CD8^{+} T cells in the lymph nodes of *Foxp3*^{cre} and *Foxp3*^{cre}*Cxxc1*$^{fl/fl}$ mice (n = 6).

All mice analyzed were 18-20 days old unless otherwise specified. Error bars show mean ± SD. The log-rank survival curve was used for survival analysis in A, and multiple unpaired *t*-test or two-tailed Student's *t*-test were used for statistical analyses in B, E, Gand H (***P*<0.01, ****P*□<□0.001, *****P*<0.0001). The flow cytometry results are representative of three independent experiments.

Fig. 4. CXXC1 is essential for T_{reg} cells to suppress T cell-mediated EAE and colitis.

(**A**)Mean clinical scores for EAE in *Rag1*$^{-/-}$ recipients of 2D2 CD4^{+} T cells, either alone or in combination with *Foxp3*^{cre} or *Foxp3*^{cre}*Cxxc1*$^{fl/fl}$ mice after immunization with MOG35–55, complete Freund's adjuvant (CFA), and pertussis toxin (n=5).

(**B** and **C**)Representative histology of the spinal cord of *Rag1*$^{-/-}$ mice after EAE induction. Hematoxylin and eosin(H&E) staining (upper), Luxol fast blue (F&B) staining (lower). Scale bars, 50 μm (400×) and 200 μm (100×).

(**D**)Representative flow cytometry plots and quantification of the the percentages of IFNγ^{+} or IL-17A^{+} CD4^{+}Vβ11^{+} T cells (n=5).

(**E**)Statistical analysis of the percentage CD4^{+} FOXP3^{+} T_{reg} cell in CNS tissues 14 days after EAE induction.

(**F**)Changes in body weight of *Rag1*$^{-/-}$ mice after colitis induction(n=6).

(**G**)Haematoxylin and eosin (H&E) staining of colons from T cell-induced colitis mice 6

weeks after T cell transfer. Scale bars, 50 μm (400×) and 200 μm (100×).

(**H**)Statistical analysis of the percentage $CD4^+$ $FOXP3^+$ T_{reg} cell in the spleen, mesenteric lymph nodes, and colon 6 weeks after colitis induction.

Error bars show mean ± SD. *P* values are determined by a two-tailed Student's *t*-test or two-way ANOVA and Holm–Sidak post hoc test (A, D, E and H). (**P*<0.05, ***P*<0.01, ****P*<0.001, *****P*<0.0001).

Fig. 5. Single-cell transcriptomics reveals distinct T_{reg} cell populations.

(**A**)UMAP plot showing clusters identified based on variable gene expression of sorted $CD4^+YFP^+$ T_{reg} cells. Each dot represents a cell, and each color corresponds to a different population of cell types. Clustering analysis revealed 8 distinct T_{reg} cell populations.

(**B**)Mean fold changes in cluster abundance between *Foxp3*^{cre} and *Foxp3*^{cre}*Cxxc1*$^{fl/fl}$ mice.

(**C**)Pseudotime trajectories of T_{reg} cells based on Slingshot, color-coded by T_{reg} cell subpopulations.

(**D**)Visualization of density and clonotype richness across T_{reg} clusters from *Foxp3*^{cre} and *Foxp3*^{cre}*Cxxc1*$^{fl/fl}$ mice.

(**E**)TCR sharing of expanded clonotypes across all possible combinations of T_{reg} cells from *Foxp3*^{cre} and *Foxp3*^{cre}*Cxxc1*$^{fl/fl}$ mice.

(**F**)Heatmap showing Z scores for the average expression of T_{reg}-specific genes in each cluster between *Foxp3*^{cre} and *Foxp3*^{cre}*Cxxc1*$^{fl/fl}$ mice.

(**G-H**)Representative flow cytometry plots and quantification of (G) expression of CD25, CD69, ICOS, T-bet, and (H) IFN-γ in $CD4^+YFP^+$ T_{reg} cells from *Foxp3*^{cre} and *Foxp3*^{cre}*Cxxc1*$^{fl/fl}$ mice (n=5 CD25, n=10 CD69, n=5 ICOS, n=6 T-bet, n=5

IFN-γ).

(**I**)Ki-67 expression (left) and frequency (right) in $CD4^{+}FOXP3^{+}$ T_{reg} cells from *Foxp3* ^{cre} a-nd *Foxp3*^{cre}*Cxxc1*$^{fl/fl}$ mice (n=6).

Error bars show mean ± SD. *P* values are determined by a two-tailed Student's *t*-test (G-I). (***P*<0.01, ****P*□<□0.001, *****P*<0.0001). The flow cytometry results are representative of three independent experiments.

Fig. 6. *Cxxc1*-deficient T_{reg} cells exhibit functional impairment and disrupted homeostasis in steady-state conditions.

(**A**)Schematic representation of wild-type and Cre-positive T_{reg} cells in female *Foxp3*$^{Cre/+}$mice.

(**B**)Flow cytometry analysis of the $YFP^{-}FOXP3^{+}$ (WT) and $YFP^{+}FOXP3^{+}$ (KO) T_{reg} cells in *Foxp3*$^{Cre/+}$ *Cxxc1*$^{fl/+}$ (het-WT) and *Foxp3*$^{Cre/+}$ *Cxxc1*$^{fl/fl}$ (het-KO) female mice (left), along with the frequency and absolute numbers of YFP^{+} cells within the total T_{reg} population (right)(n=5).

(**C**)Flow cytometry analysis of Ki-67expression (left) and MFI (right) in YFP^{-} and YFP^{+} cells within the $CD4^{+}FOXP3^{+}$ T_{reg} cells from 6- to 8-week-old het-KO female mice (n=4).

(**D**)Representative flow cytometry plots and quantification of ICOS, CD25, CTLA4, and GITR expression in YFP^{-} and YFP^{+} cells within $CD4^{+}FOXP3^{+}$ T_{reg} cells from het-KO female mice (n=5).

(E) Suppression of CFSE-labelled Tn cell proliferation by different ratios of $CD4^{+}YFP^{+}$ T_{reg} cells from *Foxp3*$^{Cre/+}$ *Cxxc1*$^{fl/+}$ and *Foxp3*$^{Cre/+}$ *Cxxc1*$^{fl/fl}$ female mice. On the right, the percentage of proliferated responding T cells is presented (n=5).

Error bars show mean ± SD. *P* values are determined by a two-tailed Student's *t*-test (B-E). (ns, not significant. *$P<0.05$,**$P<0.01$, ***$P<0.001$, ****$P<0.0001$). The flow cytometry results are representative of three independent experiments.

Fig. 7. CXXC1 regulates Foxp3-dependent molecule H3K4 trimethylation in T_{reg} cells.

(**A**-**B**)Heatmaps showing H3K4me3(A)and CXXC1(B) signals centered on narrow, medium, and broad domains. The top panel shows the average CUT&Tag signals around indicated domains.

(**C**)Venn diagrams showing the overlap of FOXP3 binding genes, CXXC1 binding genes, and H3K4me3-BD-associated genes with decreased H3K4me3 levels after CXXC1 depletion in T_{reg} cells.

(**D**)Gene Ontology (GO) pathway analysis of the overlap peaks.

(**E**)Representative genome browser view showing the enrichments of FOXP3, CXXC1, and H3K4me3 in T_{reg} cells.

References

1 Sakaguchi, S., Yamaguchi, T., Nomura, T. & Ono, M. Regulatory T cells and immune tolerance. Cell 133, 775-787, doi:10.1016/j.cell.2008.05.009 (2008).

2 Josefowicz, S. Z., Lu, L. F. & Rudensky, A. Y. in *Annual Review of Immunology, Vol 30* Vol. 30 *Annual Review of Immunology* (ed W. E. Paul) 531-564 (2012).

3 Singer, B. D., King, L. S. & D'Alessio, F. R. Regulatory T cells as immunotherapy. Frontiers in Immunology 5, doi:10.3389/fimmu.2014.00046 (2014).

4 Ohkura, N. & Sakaguchi, S. Transcriptional and epigenetic basis of Treg cell development and function: its genetic anomalies or variations in autoimmune diseases. Cell Research 30, 465-474, doi:10.1038/s41422-020-0324-7 (2020).

5 Littman, D. R. & Rudensky, A. Y. Th17 and Regulatory T Cells in Mediating and Restraining Inflammation. Cell 140, 845-858, doi:10.1016/j.cell.2010.02.021 (2010).

6 Sakaguchi, S., Vignali, D. A. A., Rudensky, A. Y., Niec, R. E. & Waldmann, H. The plasticity and stability of regulatory T cells. Nature Reviews Immunology 13, 461-467, doi:10.1038/nri3464 (2013).

7 Fontenot, J. D., Gavin, M. A. & Rudensky, A. Y. Foxp3 programs the development and function of CD4+CD25+ regulatory T cells. Nat Immunol 4, 330-336, doi:10.1038/ni904 (2003).

8 Van Gool, F., Nguyen, M. L. T., Mumbach, M. R., Satpathy, A. T., Rosenthal, W. L., Giacometti, S., Le, D. T., Liu, W., Brusko, T. M., Anderson, M. S., Rudensky, A. Y., Marson, A., Chang, H. Y. & Bluestone, J. A. A Mutation in the Transcription Factor Foxp3 Drives T

Helper 2 Effector Function in Regulatory T Cells. Immunity 50, 362-+, doi:10.1016/j.immuni.2018.12.016 (2019).

9 Katoh, H., Qin, Z. S., Liu, R., Wang, L., Li, W., Li, X., Wu, L., Du, Z., Lyons, R., Liu, C.-G., Liu, X., Dou, Y., Zheng, P. & Liu, Y. FOXP3 Orchestrates H4K16 Acetylation and H3K4 Trimethylation for Activation of Multiple Genes by Recruiting MOF and Causing Displacement of PLU-1. Molecular Cell 44, 770-784, doi:10.1016/j.molcel.2011.10.012 (2011).

10 Wang, L., Liu, Y., Han, R., Beier, U. H., Bhatti, T. R., Akimova, T., Greene, M. I., Hiebert, S. W. & Hancock, W. W. FOXP3(+) regulatory T cell development and function require histone/protein deacetylase 3. Journal of Clinical Investigation 125, 1111-1123, doi:10.1172/jci77088 (2015).

11 Arvey, A., van der Veeken, J., Samstein, R. M., Feng, Y., Stamatoyannopoulos, J. A. & Rudensky, A. Y. Inflammation-induced repression of chromatin bound by the transcription factor Foxp3 in regulatory T cells. Nature Immunology 15, 580-587, doi:10.1038/ni.2868 (2014).

12 Ruthenburg, A. J., Allis, C. D. & Wysocka, J. Methylation of lysine 4 on histone H3: Intricacy of writing and reading a single epigenetic mark. Molecular Cell 25, 15-30, doi:10.1016/j.molcel.2006.12.014 (2007).

13 Takahashi, Y.-h., Westfield, G. H., Oleskie, A. N., Trievel, R. C., Shilatifard, A. & Skiniotis, G. Structural analysis of the core COMPASS family of histone H3K4 methylases from yeast to human. Proceedings of the National Academy of Sciences of the United States of America 108, 20526-20531, doi:10.1073/pnas.1109360108 (2011).

14 Wang, T., Guo, J., Li, L., Jin, Q., Zhang, F., Hou, B., Zhang, Y. & Zhou, X. The histone lysine methyltransferase MLL1 regulates the activation and functional specialization of regulatory T cells. Cell Reports 43, doi:10.1016/j.celrep.2024.114222 (2024).

15 Placek, K., Hu, G., Cui, K., Zhang, D., Ding, Y., Lee, J.-E., Jang, Y., Wang, C., Konkel, J. E., Song, J., Liu, C., Ge, K., Chen, W. & Zhao, K. MLL4 prepares the enhancer landscape for Foxp3 induction via chromatin looping. Nature Immunology 18, 1035-+, doi:10.1038/ni.3812 (2017).

16 Yang, Y., Yang, Y., Chan, K. & Couture, J.-F. Analyzing the impact of CFP1 mutational landscape on epigenetic signaling. Faseb Journal 35, doi:10.1096/fj.202100427R (2021).

17 Tate, C. M., Lee, J.-H. & Skalnik, D. G. CXXC finger protein 1 restricts the Setd1A histone H3K4 methyltransferase complex to euchromatin. Febs Journal 277, 210-223, doi:10.1111/j.1742-4658.2009.07475.x (2010).

18 Cao, W., Guo, J., Wen, X., Miao, L., Lin, F., Xu, G., Ma, R., Yin, S., Hui, Z., Chen, T., Guo, S., Chen, W., Huang, Y., Liu, Y., Wang, J., Wei, L. & Wang, L. CXXC finger protein 1 is critical for T-cell intrathymic development through regulating H3K4 trimethylation. Nat Commun 7, 11687, doi:10.1038/ncomms11687 (2016).

19 Hui, Z., Zhou, L., Xue, Z., Zhou, L., Luo, Y., Lin, F., Liu, X., Hong, S., Li, W., Wang, D., Lu, L., Wang, J. & Wang, L. Cxxc Finger Protein 1 Positively Regulates GM-CSF-Derived Macrophage Phagocytosis Through Csf2rα-Mediated Signaling. Frontiers in Immunology 9, doi:10.3389/fimmu.2018.01885 (2018).

20 Lin, F., Meng, X., Guo, Y., Cao, W., Liu, W., Xia, Q., Hui, Z., Chen, J., Hong, S., Zhang, X., Wu, C., Wang, D., Wang, J., Lu, L., Qian, W., Wei, L. & Wang, L. Epigenetic initiation of

the T(H)17 differentiation program is promoted by Cxxc finger protein 1. Science Advances 5, doi:10.1126/sciadv.aax1608 (2019).

21 Shen, X., Gao, X., Luo, Y., Xu, Q., Fan, Y., Hong, S., Huang, Z., Liu, X., Wang, Q., Chen, Z., Wang, D., Lu, L., Wu, C., Liang, H. & Wang, L. Cxxc finger protein 1 maintains homeostasis and function of intestinal group 3 innate lymphoid cells with aging. Nature Aging 3, 965-+, doi:10.1038/s43587-023-00453-7 (2023).

22 Cao, W., Guo, J., Wen, X., Miao, L., Lin, F., Xu, G., Ma, R., Yin, S., Hui, Z., Chen, T., Guo, S., Chen, W., Huang, Y., Liu, Y., Wang, J., Wei, L. & Wang, L. CXXC finger protein 1 is critical for T-cell intrathymic development through regulating H3K4 trimethylation. Nature Communications 7, doi:10.1038/ncomms11687 (2016).

23 Zhou, L., Wang, S., Hu, W., Liu, X., Xu, L., Tong, B., Zhang, T., Xue, Z., Guo, Y., Zhao, J., Lu, L., Fan, H., Qian, W., Chen, J., Chen, W. & Wang, L. T cell proliferation requires ribosomal maturation in nucleolar condensates dependent on DCAF13. Journal of Cell Biology 222, doi:10.1083/jcb.202201096 (2023).

24 Chou, W.-C., Guo, Z., Guo, H., Chen, L., Zhang, G., Liang, K., Xie, L., Tan, X., Gibson, S. A., Rampanelli, E., Wang, Y., Montgomery, S. A., Brickey, W. J., Deng, M., Freeman, L., Zhang, S., Su, M. A., Chen, X., Wan, Y. Y. & Ting, J. P. Y. AIM2 in regulatory T cells restrains autoimmune diseases. Nature 591, 300-+, doi:10.1038/s41586-021-03231-w (2021).

25 Zeng, H., Yang, K., Cloer, C., Neale, G., Vogel, P. & Chi, H. mTORC1 couples immune signals and metabolic programming to establish T(reg)-cell function. Nature 499, 485-490, doi:10.1038/nature12297 (2013).

26 Lu, D., Liu, L., Sun, Y., Song, J., Yin, Q., Zhang, G., Qi, F., Hu, Z., Yang, Z., Zhou, Z.,

Hu, Y., Zhang, L., Ji, J., Zhao, X., Jin, Y., McNutt, M. A. & Yin, Y. The phosphatase PAC1 acts as a T cell suppressor and attenuates host antitumor immunity. Nature Immunology 21, 287-+, doi:10.1038/s41590-019-0577-9 (2020).

27 Chen, J., Liu, K., Luo, Y., Kang, M., Wang, J., Chen, G., Qi, J., Wu, W., Wang, B., Han, Y., Shi, L., Wang, K., Han, X., Ma, X., Liu, W., Ding, Y., Wang, L., Liang, H., Wang, L. & Chen, J. Single-Cell Profiling of Tumor Immune Microenvironment Reveals Immune Irresponsiveness in Gastric Signet-Ring Cell Carcinoma. Gastroenterology 165, 88-103, doi:10.1053/j.gastro.2023.03.008 (2023).

28 Marson, A., Kretschmer, K., Frampton, G. M., Jacobsen, E. S., Polansky, J. K., Maclsaac, K. D., Levine, S. S., Fraenkel, E., von Boehmer, H. & Young, R. A. Foxp3 occupancy and regulation of key target genes during T-cell stimulation. Nature 445, 931-935, doi:10.1038/nature05478 (2007).

29 Zheng, Y., Josefowicz, S. Z., Kas, A., Chu, T.-T., Gavin, M. A. & Rudensky, A. Y. Genome-wide analysis of Foxp3 target genes in developing and mature regulatory T cells. Nature 445, 936-940, doi:10.1038/nature05563 (2007).

30 Ono, M., Yaguchi, H., Ohkura, N., Kitabayashi, I., Nagamura, Y., Nomura, T., Miyachi, Y., Tsukada, T. & Sakaguchi, S. Foxp3 controls regulatory T-cell function by interacting with AML1/Runx1. Nature 446, 685-689, doi:10.1038/nature05673 (2007).

31 Fu, W., Ergun, A., Lu, T., Hill, J. A., Haxhinasto, S., Fassett, M. S., Gazit, R., Adoro, S., Glimcher, L., Chan, S., Kastner, P., Rossi, D., Collins, J. J., Mathis, D. & Benoist, C. A multiply redundant genetic switch 'locks in' the transcriptional signature of regulatory T cells. Nature Immunology 13, 972-980, doi:10.1038/ni.2420 (2012).

32 Ohkura, N., Hamaguchi, M., Morikawa, H., Sugimura, K., Tanaka, A., Ito, Y., Osaki, M., Tanaka, Y., Yamashita, R., Nakano, N., Huehn, J., Fehling, H. J., Sparwasser, T., Nakai, K. & Sakaguchi, S. T Cell Receptor Stimulation-Induced Epigenetic Changes and Foxp3 Expression Are Independent and Complementary Events Required for Treg Cell Development. Immunity 37, 785-799, doi:10.1016/j.immuni.2012.09.010 (2012).

33 Wei, G., Wei, L., Zhu, J., Zang, C., Hu-Li, J., Yao, Z., Cui, K., Kanno, Y., Roh, T.-Y., Watford, W. T., Schones, D. E., Peng, W., Sun, H.-w., Paul, W. E., O'Shea, J. J. & Zhao, K. Global Mapping of H3K4me3 and H3K27me3 Reveals Specificity and Plasticity in Lineage Fate Determination of Differentiating CD4(+) T Cells. Immunity 30, 155-167, doi:10.1016/j.immuni.2008.12.009 (2009).

34 Konopacki, C., Pritykin, Y., Rubtsov, Y., Leslie, C. S. & Rudensky, A. Y. Transcription factor Foxp1 regulates Foxp3 chromatin binding and coordinates regulatory T cell function. Nature Immunology 20, 232-+, doi:10.1038/s41590-018-0291-z (2019).

35 Hill, J. A., Feuerer, M., Tash, K., Haxhinasto, S., Perez, J., Melamed, R., Mathis, D. & Benoist, C. Foxp3 transcription-factor-dependent and -independent regulation of the regulatory T cell transcriptional signature. Immunity 27, 786-800, doi:10.1016/j.immuni.2007.09.010 (2007).

36 Oh, H., Grinberg-Bleyer, Y., Liao, W., Maloney, D., Wang, P., Wu, Z., Wang, J., Bhatt, D. M., Heise, N., Schmid, R. M., Hayden, M. S., Klein, U., Rabadan, R. & Ghosh, S. An NF-kappaB Transcription-Factor-Dependent Lineage-Specific Transcriptional Program Promotes Regulatory T Cell Identity and Function. Immunity 47, 450-465 e455, doi:10.1016/j.immuni.2017.08.010 (2017).

37 Rubtsov, Y. P., Rasmussen, J. P., Chi, E. Y., Fontenot, J., Castelli, L., Ye, X., Treuting, P., Siewe, L., Roers, A., Henderson, W. R., Jr., Muller, W. & Rudensky, A. Y. Regulatory T cell-derived interleukin-10 limits inflammation at environmental interfaces. Immunity 28, 546-558, doi:10.1016/j.immuni.2008.02.017 (2008).

38 Fontenot, J. D., Gavin, M. A. & Rudensky, A. Y. Foxp3 programs the development and function of CD4(+)CD25(+) regulatory T cells. Nature Immunology 4, 330-336, doi:10.1038/ni904 (2003).

39 Kim, J. M., Rasmussen, J. P. & Rudensky, A. Y. Regulatory T cells prevent catastrophic autoimmunity throughout the lifespan of mice. Nature Immunology 8, 191-197, doi:10.1038/ni1428 (2007).

40 Shevyrev, D. & Tereshchenko, V. Treg Heterogeneity, Function, and Homeostasis. Frontiers in Immunology 10, doi:10.3389/fimmu.2019.03100 (2020).

41 Zagorulya, M., Yim, L., Morgan, D. M., Edwards, A., Torres-Mejia, E., Momin, N., McCreery, C. V., Zamora, I. L., Horton, B. L., Fox, J. G., Wittrup, K. D., Love, J. C. & Spranger, S. Tissue-specific abundance of interferon-gamma drives regulatory T cells to restrain DC1-mediated priming of cytotoxic T cells against lung cancer. Immunity 56, 386-+, doi:10.1016/j.immuni.2023.01.010 (2023).

42 Dikiy, S. & Rudensky, A. Y. Principles of regulatory T cell function. Immunity 56, 240-255, doi:10.1016/j.immuni.2023.01.004 (2023).

43 Street, K., Risso, D., Fletcher, R. B., Das, D., Ngai, J., Yosef, N., Purdom, E. & Dudoit, S. Slingshot: cell lineage and pseudotime inference for single-cell transcriptomics. Bmc Genomics 19, doi:10.1186/s12864-018-4772-0 (2018).

44 Tarbell, K. V., Yamazaki, S., Olson, K., Toy, P. & Steinman, R. M. CD25+CD4+T cells, expanded with dendritic cells presenting a single autoantigenic peptide, suppress autoimmune diabetes. Journal of Experimental Medicine 199, 1467-1477, doi:10.1084/jem.20040180 (2004).

45 Hori, S., Haury, M., Coutinho, A. & Demengeot, J. Specificity requirements for selection and effector functions of CD25+4+ regulatory T cells in anti-myelin basic protein T cell receptor transgenic mice. Proceedings of the National Academy of Sciences of the United States of America 99, 8213-8218, doi:10.1073/pnas.122224799 (2002).

46 Butler, J. S., Lee, J.-H. & Skalnik, D. G. CFP1 Interacts with DNMT1 Independently of Association with the Setd1 Histone H3K4 Methyltransferase Complexes. DNA and Cell Biology 27, 533-543, doi:10.1089/dna.2007.0714 (2008).

47 Butler, J. S., Palam, L. R., Tate, C. M., Sanford, J. R., Wek, R. C. & Skalnik, D. G. DNA Methyltransferase Protein Synthesis Is Reduced in CXXC Finger Protein 1-Deficient Embryonic Stem Cells. DNA and Cell Biology 28, 223-231, doi:10.1089/dna.2009.0854 (2009).

48 Benayoun, B. A., Pollina, E. A., Ucar, D., Mahmoudi, S., Karra, K., Wong, E. D., Devarajan, K., Daugherty, A. C., Kundaje, A. B., Mancini, E., Hitz, B. C., Gupta, R., Rando, T. A., Baker, J. C., Snyder, M. P., Cherry, J. M. & Brunet, A. H3K4me3 Breadth Is Linked to Cell Identity and Transcriptional Consistency. Cell 158, 673-688, doi:10.1016/j.cell.2014.06.027 (2014).

49 Zacarias-Cabeza, J., Belhocine, M., Vanhille, L., Cauchy, P., Koch, F., Pekowska, A., Fenouil, R., Bergon, A., Gut, M., Gut, I., Eick, D., Imbert, J., Ferrier, P., Andrau, J.-C. &

Spicuglia, S. Transcription-Dependent Generation of a Specialized Chromatin Structure at the TCRβ Locus. Journal of Immunology 194, 3432-3443, doi:10.4049/jimmunol.1400789 (2015).

50 Chen, K., Chen, Z., Wu, D., Zhang, L., Lin, X., Su, J., Rodriguez, B., Xi, Y., Xia, Z., Chen, X., Shi, X., Wang, Q. & Li, W. Broad H3K4me3 is associated with increased transcription elongation and enhancer activity at tumor-suppressor genes. Nature Genetics 47, 1149-+, doi:10.1038/ng.3385 (2015).

51 Zhang, R., Huynh, A., Whitcher, G., Chang, J., Maltzman, J. S. & Turka, L. A. An obligate cell-intrinsic function for CD28 in Tregs. Journal of Clinical Investigation 123, 580-593, doi:10.1172/jci65013 (2013).

52 Gokhale, A. S., Gangaplara, A., Lopez-Occasio, M., Thornton, A. M. & Shevach, E. M. Selective deletion of Eos (Ikzf4) in T-regulatory cells leads to loss of suppressive function and development of systemic autoimmunity. Journal of Autoimmunity 105, doi:10.1016/j.jaut.2019.06.011 (2019).

53 Wan, Y. Y. & Flavell, R. A. Regulatory T-cell functions are subverted and converted owing to attenuated Foxp3 expression. Nature 445, 766-770, doi:10.1038/nature05479 (2007).

54 Chen, C., Rowell, E. A., Thomas, R. M., Hancock, W. W. & Wells, A. D. Transcriptional regulation by Foxp3 is associated with direct promoter occupancy and modulation of histone acetylation. Journal of Biological Chemistry 281, 36828-36834, doi:10.1074/jbc.M608848200 (2006).

55 Morikawa, H., Ohkura, N., Vandenbon, A., Itoh, M., Nagao-Sato, S., Kawaji, H.,

Lassmann, T., Carninci, P., Hayashizaki, Y., Forrest, A. R. R., Standley, D. M., Date, H., Sakaguchi, S. & Consortium, F. Differential roles of epigenetic changes and Foxp3 expression in regulatory T cell-specific transcriptional regulation. Proceedings of the National Academy of Sciences of the United States of America 111, 5289-5294, doi:10.1073/pnas.1312717110 (2014).

56 Pan, F., Yu, H., Dang, E. V., Barbi, J., Pan, X., Grosso, J. F., Jinasena, D., Sharma, S. M., McCadden, E. M., Getnet, D., Drake, C. G., Liu, J. O., Ostrowski, M. C. & Pardoll, D. M. Eos Mediates Foxp3-Dependent Gene Silencing in CD4+ Regulatory T Cells. Science 325, 1142-1146, doi:10.1126/science.1176077 (2009).

57 DuPage, M., Chopra, G., Quiros, J., Rosenthal, W. L., Morar, M. M., Holohan, D., Zhang, R., Turka, L., Marson, A. & Bluestone, J. A. The Chromatin-Modifying Enzyme Ezh2 Is Critical for the Maintenance of Regulatory T Cell Identity after Activation. Immunity 42, 227-238, doi:10.1016/j.immuni.2015.01.007 (2015).

58 Liu, X., Wang, C., Liu, W., Li, J., Li, C., Kou, X., Chen, J., Zhao, Y., Gao, H., Wang, H., Zhang, Y., Gao, Y. & Gao, S. Distinct features of H3K4me3 and H3K27me3 chromatin domains in pre-implantation embryos. Nature 537, 558-+, doi:10.1038/nature19362 (2016).

59 Sze, C. C., Ozark, P. A., Cao, K., Ugarenko, M., Das, S., Wang, L., Marshall, S. A., Rendleman, E. J., Ryan, C. A., Zha, D., Douillet, D., Chen, F. X. & Shilatifard, A. Coordinated regulation of cellular identity-associated H3K4me3 breadth by the COMPASS family. Science Advances 6, doi:10.1126/sciadv.aaz4764 (2020).

60 Dahl, J. A., Jung, I., Aanes, H., Greggains, G. D., Manaf, A., Lerdrup, M., Li, G., Kuan, S., Li, B., Lee, A. Y., Preissl, S., Jermstad, I., Haugen, M. H., Suganthan, R., Bjoras, M.,

Hansen, K., Dalen, K. T., Fedorcsak, P., Ren, B. & Klungland, A. Broad histone H3K4me3 domains in mouse oocytes modulate maternal-to-zygotic transition. Nature 537, 548-+, doi:10.1038/nature19360 (2016).

61 Zhang, B., Zheng, H., Huang, B., Li, W., Xiang, Y., Peng, X., Ming, J., Wu, X., Zhang, Y., Xu, Q., Liu, W., Kou, X., Zhao, Y., He, W., Li, C., Chen, B., Li, Y., Wang, Q., Ma, J., Yin, Q., Kee, K., Meng, A., Gao, S., Xu, F., Na, J. & Xie, W. Allelic reprogramming of the histone modification H3K4me3 in early mammalian development. Nature 537, 553-+, doi:10.1038/nature19361 (2016).

62 Zhang, Z., Shi, L., Dawany, N., Kelsen, J., Petri, M. A. & Sullivan, K. E. H3K4 tri-methylation breadth at transcription start sites impacts the transcriptome of systemic lupus erythematosus. Clinical Epigenetics 8, doi:10.1186/s13148-016-0179-4 (2016).

63 Wong, S. H. K., Goode, D. L., Iwasaki, M., Wei, M. C., Kuo, H.-P., Zhu, L., Schneidawind, D., Duque-Afonso, J., Weng, Z. & Cleary, M. L. The H3K4-Methyl Epigenome Regulates Leukemia Stem Cell Oncogenic Potential. Cancer Cell 28, 198-209, doi:10.1016/j.ccell.2015.06.003 (2015).

64 Deaglio, S., Dwyer, K. M., Gao, W., Friedman, D., Usheva, A., Erat, A., Chen, J.-F., Enjyoji, K., Linden, J., Oukka, M., Kuchroo, V. K., Strom, T. B. & Robson, S. C. Adenosine generation catalyzed by CD39 and CD73 expressed on regulatory T cells mediates immune suppression. Journal of Experimental Medicine 204, 1257-1265, doi:10.1084/jem.20062512 (2007).

65 Lee, J. H. & Skalnik, D. G. CpG-binding protein (CXXC finger protein 1) is a component of the mammalian set1 histone H3-Lys4 methyltransferase complex, the analogue of the yeast

Set1/COMPASS complex. Journal of Biological Chemistry 280, 41725-41731, doi:10.1074/jbc.M508312200 (2005).

66 Thomson, J. P., Skene, P. J., Selfridge, J., Clouaire, T., Guy, J., Webb, S., Kerr, A. R. W., Deaton, A., Andrews, R., James, K. D., Turner, D. J., Illingworth, R. & Bird, A. CpG islands influence chromatin structure via the CpG-binding protein Cfp1. Nature 464, 1082-U1162, doi:10.1038/nature08924 (2010).

67 Shilatifard, A. in *Annual Review of Biochemistry, Vol 81* Vol. 81 *Annual Review of Biochemistry* (ed R. D. Kornberg) 65-95 (2012).

68 Brown, D. A., Di Cerbo, V., Feldmann, A., Ahn, J., Ito, S., Blackledge, N. P., Nakayama, M., McClellan, M., Dimitrova, E., Turberfield, A. H., Long, H. K., King, H. W., Kriaucionis, S., Schermelleh, L., Kutateladze, T. G., Koseki, H. & Klose, R. J. The SET1 Complex Selects Actively Transcribed Target Genes via Multivalent Interaction with CpG Island Chromatin. Cell Reports 20, 2313-2327, doi:10.1016/j.celrep.2017.08.030 (2017).

Fig.1

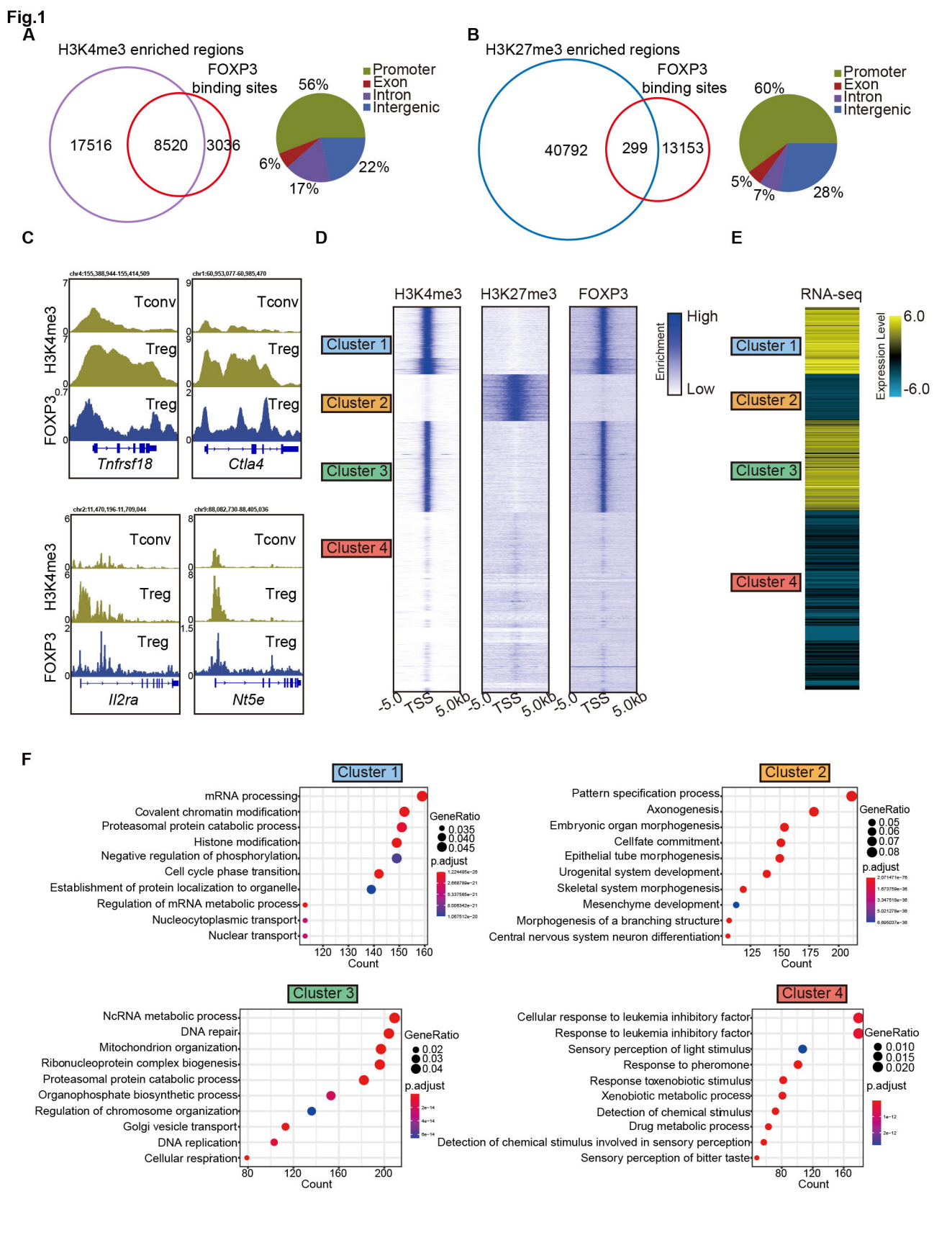
A
H3K4me3 enriched regions
FOXP3 binding sites
17516
8520
3036
Promoter
Exon
Intron
Intergenic
56%
6%
17%
22%
B
H3K27me3 enriched regions
FOXP3 binding sites
40792
299
13153
60%
5%
7%
28%
C
Tconv
Treg
H3K4me3
FOXP3
Tnfrsf18
Ctla4
Il2ra
Nt5e
D
H3K4me3
H3K27me3
FOXP3
Cluster 1
Cluster 2
Cluster 3
Cluster 4
Enrichment
High
Low
-5.0
TSS
5.0kb
E
RNA-seq
Expression Level
6.0
-6.0
F
Cluster 1
mRNA processing
Covalent chromatin modification
Proteasomal protein catabolic process
Histone modification
Negative regulation of phosphorylation
Cell cycle phase transition
Establishment of protein localization to organelle
Regulation of mRNA metabolic process
Nucleocytoplasmic transport
Nuclear transport
GeneRatio
p.adjust
Count
Cluster 2
Pattern specification process
Axonogenesis
Embryonic organ morphogenesis
Cellfate commitment
Epithelial tube morphogenesis
Urogenital system development
Skeletal system morphogenesis
Mesenchyme development
Morphogenesis of a branching structure
Central nervous system neuron differentiation
Cluster 3
NcRNA metabolic process
DNA repair
Mitochondrion organization
Ribonucleoprotein complex biogenesis
Proteasomal protein catabolic process
Organophosphate biosynthetic process
Regulation of chromosome organization
Golgi vesicle transport
DNA replication
Cellular respiration
Cluster 4
Cellular response to leukemia inhibitory factor
Response to leukemia inhibitory factor
Sensory perception of light stimulus
Response to pheromone
Response toxenobiotic stimulus
Xenobiotic metabolic process
Detection of chemical stimulus
Drug metabolic process
Detection of chemical stimulus involved in sensory perception
Sensory perception of bitter taste

Fig.2

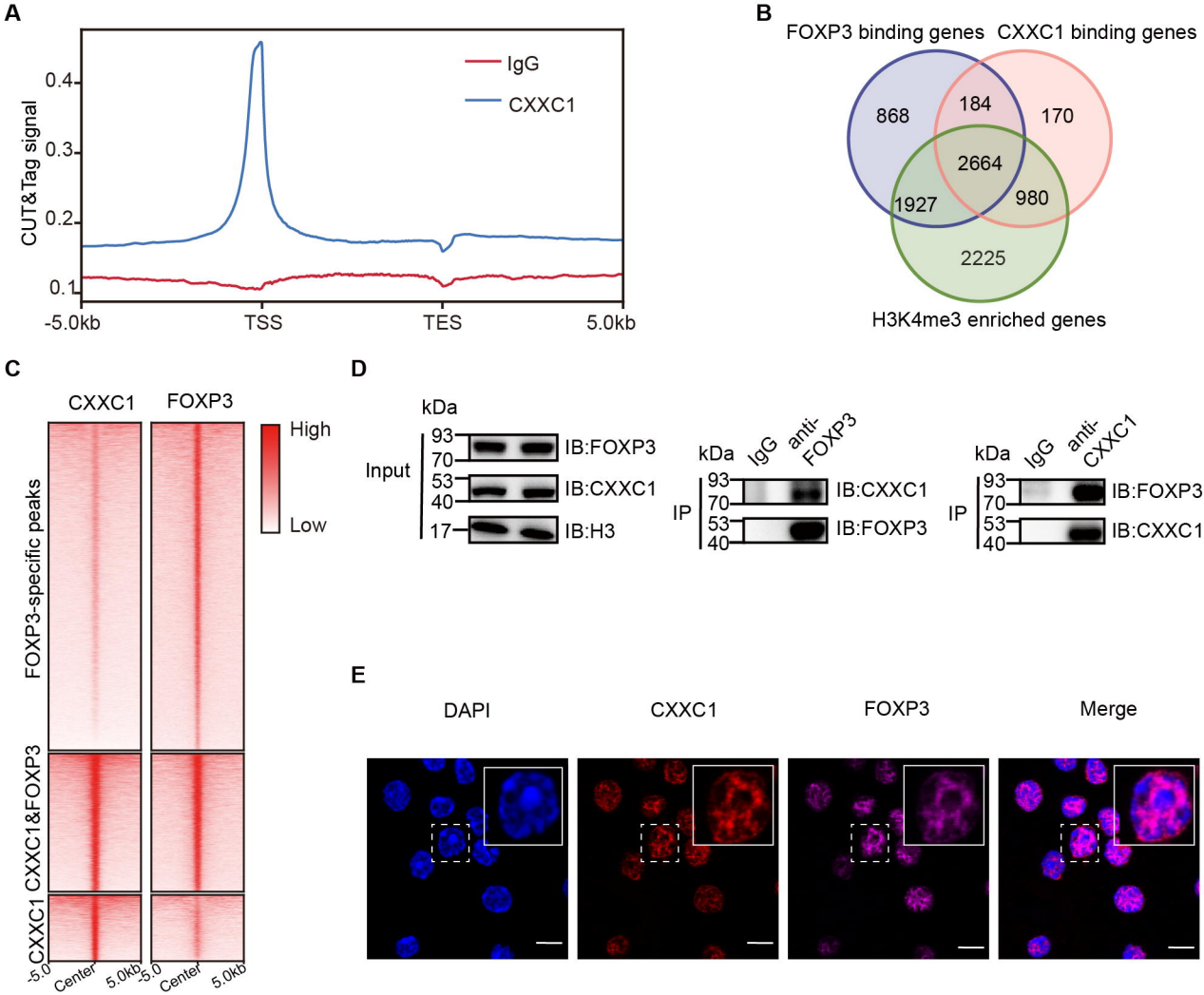
A
IgG
CXXC1
CUT&Tag signal
0.4
0.3
0.2
0.1
-5.0kb
TSS
TES
5.0kb
B
FOXP3 binding genes
CXXC1 binding genes
868
184
170
2664
1927
980
2225
H3K4me3 enriched genes
C
CXXC1
FOXP3
High
Low
FOXP3-specific peaks
CXXC1&FOXP3
CXXC1
-5.0
Center
5.0kb
D
kDa
Input
93
70
53
40
17
IB:FOXP3
IB:CXXC1
IB:H3
IgG
anti-FOXP3
IP
IB:CXXC1
IB:FOXP3
anti-CXXC1
IB:FOXP3
IB:CXXC1
E
DAPI
CXXC1
FOXP3
Merge

Fig.3

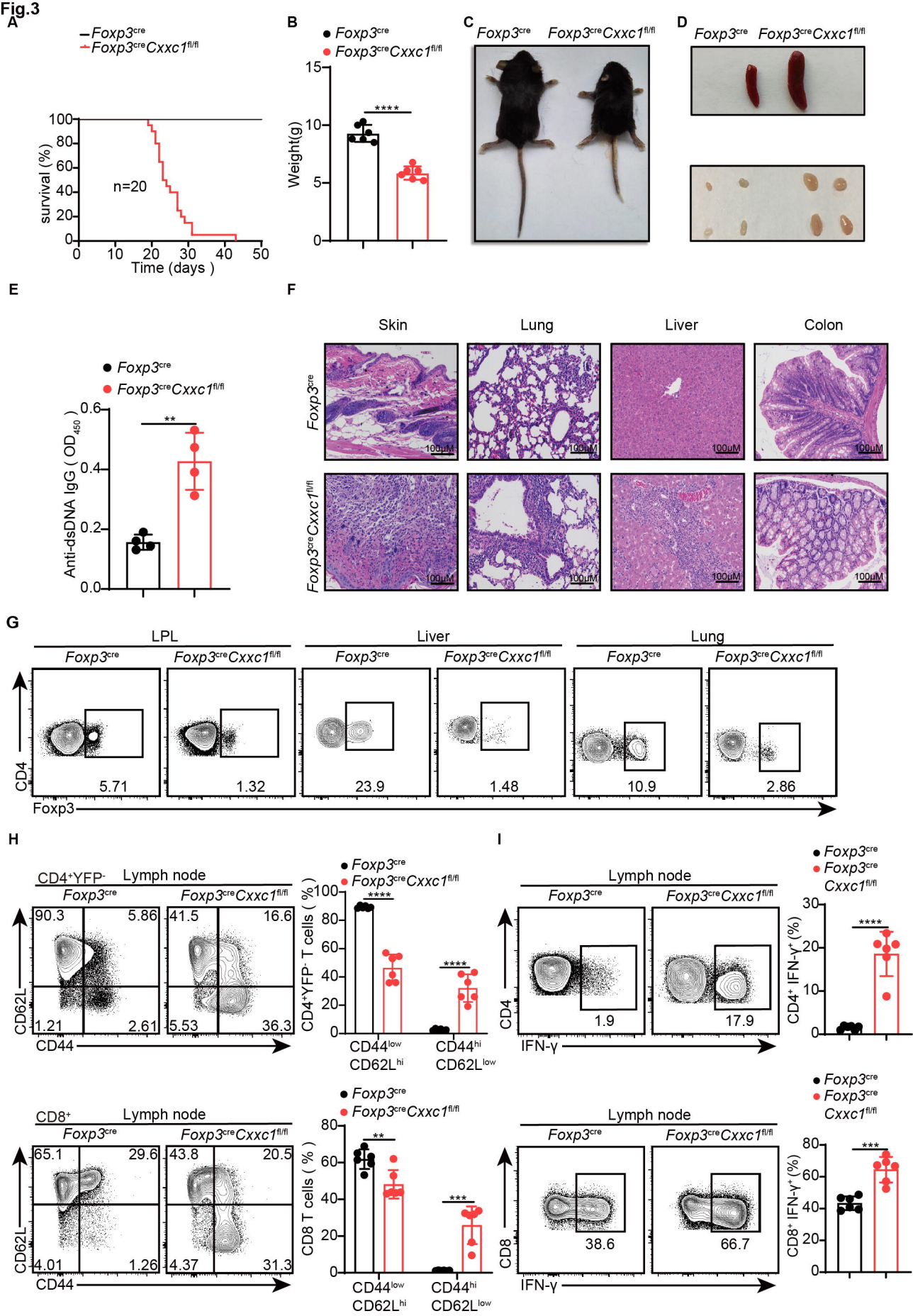
A
Foxp3cre
Foxp3creCxxc1fl/fl
survival (%)
n=20
Time (days)
B
Foxp3cre
Foxp3creCxxc1fl/fl
Weight(g)
****
C
Foxp3cre
Foxp3creCxxc1fl/fl
D
Foxp3cre
Foxp3creCxxc1fl/fl
E
Foxp3cre
Foxp3creCxxc1fl/fl
Anti-dsDNA IgG (OD450)
**
F
Skin
Lung
Liver
Colon
Foxp3cre
Foxp3creCxxc1fl/fl
100μM
G
LPL
Liver
Lung
Foxp3cre
Foxp3creCxxc1fl/fl
CD4
Foxp3
5.71
1.32
23.9
1.48
10.9
2.86
H
CD4+YFP-
Lymph node
Foxp3cre
Foxp3creCxxc1fl/fl
CD62L
CD44
90.3
5.86
1.21
2.61
41.5
16.6
5.53
36.3
CD4+YFP- T cells (%)
CD44low CD62Lhi
CD44hi CD62Llow
CD8+
65.1
29.6
4.01
1.26
43.8
20.5
4.37
31.3
CD8 T cells (%)
I
Lymph node
CD4
IFN-γ
1.9
17.9
CD4+ IFN-γ+ (%)
CD8
38.6
66.7
CD8+ IFN-γ+ (%)

Fig.4

A

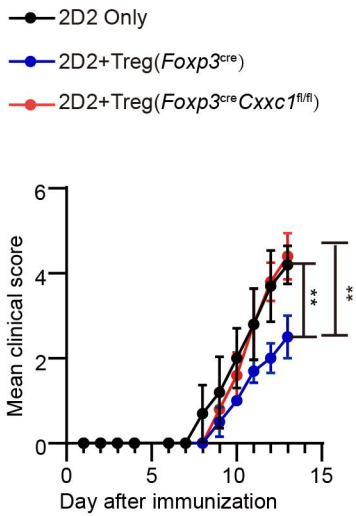

2D2 Only vs 2D2+Treg(Foxp3^{cre}), ** p=0.0013

2D2 Only vs 2D2+Treg(*Foxp3*^{cre}*Cxxc1*$^{fl/fl}$), p=ns

2D2+Treg(*Foxp3*^{cre}) vs 2D2+Treg(*Foxp3*^{cre}*Cxxc1*$^{fl/fl}$), ** p=0.0012

B

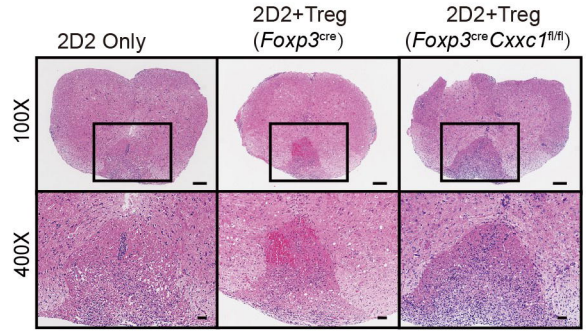

C

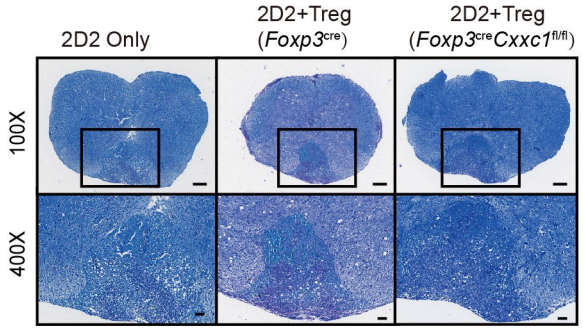

D

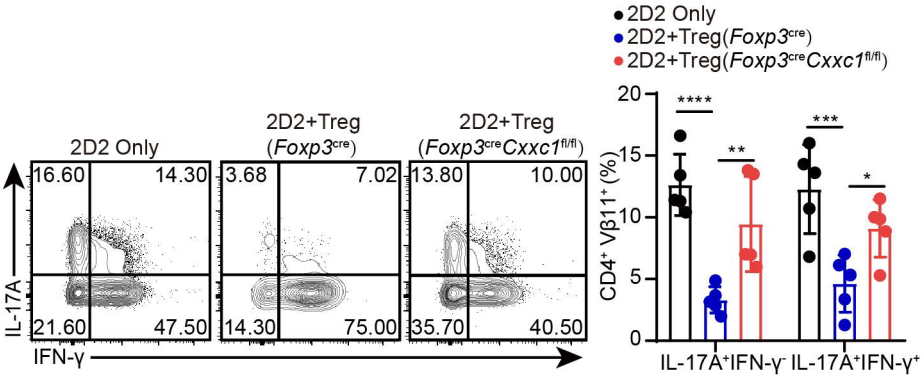

E

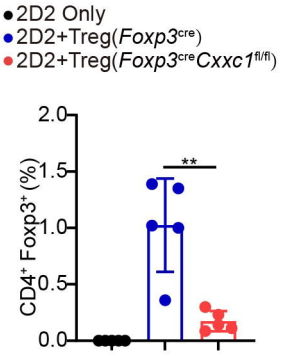

F

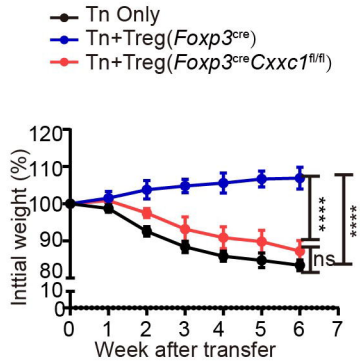

G

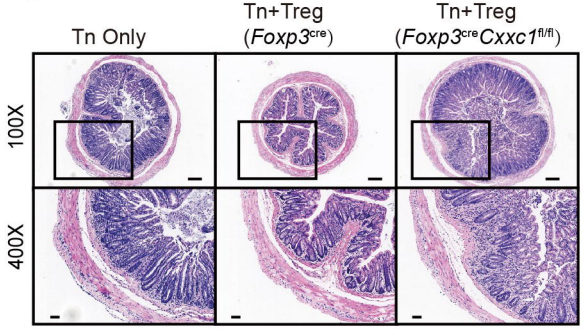

H

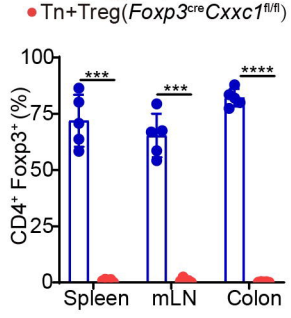

Fig.5

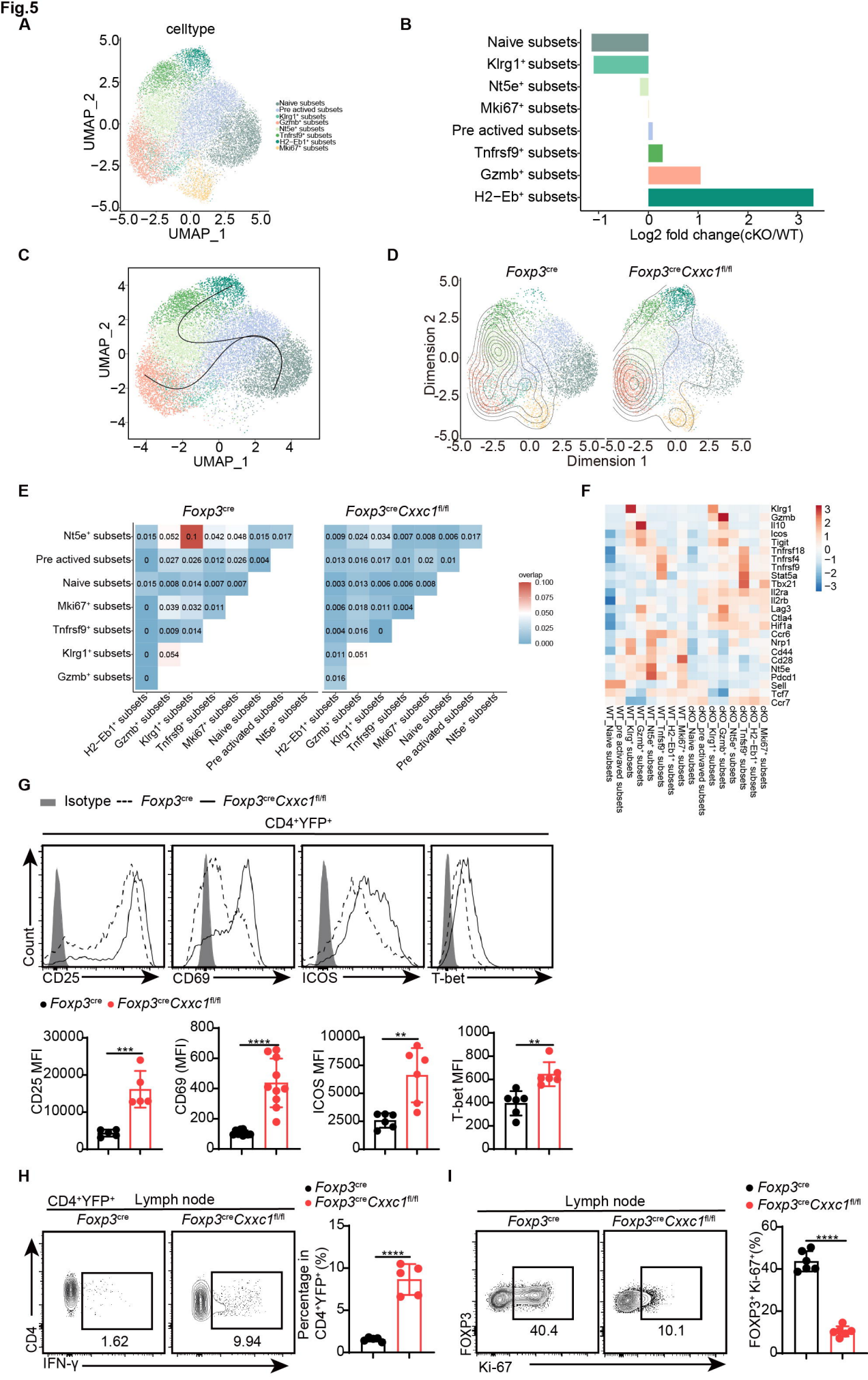
A
celltype
UMAP_2
UMAP_1
Naive subsets
Pre actived subsets
Klrg1+ subsets
Gzmb+ subsets
Nt5e+ subsets
Tnfrsf9+ subsets
H2−Eb1+ subsets
Mki67+ subsets
B
Naive subsets
Klrg1+ subsets
Nt5e+ subsets
Mki67+ subsets
Pre actived subsets
Tnfrsf9+ subsets
Gzmb+ subsets
H2−Eb+ subsets
Log2 fold change(cKO/WT)
C
UMAP_2
UMAP_1
D
Foxp3cre
Foxp3creCxxc1fl/fl
Dimension 2
Dimension 1
E
Foxp3cre
Foxp3creCxxc1fl/fl
Nt5e+ subsets
Pre actived subsets
Naive subsets
Mki67+ subsets
Tnfrsf9+ subsets
Klrg1+ subsets
Gzmb+ subsets
H2−Eb1+ subsets
Gzmb+ subsets
Klrg1+ subsets
Tnfrsf9+ subsets
Mki67+ subsets
Naive subsets
Pre activated subsets
Nt5e+ subsets
overlap
F
Klrg1
Gzmb
Il10
Icos
Tigit
Tnfrsf18
Tnfrsf4
Tnfrsf9
Stat5a
Tbx21
Il2ra
Il2rb
Lag3
Ctla4
Hif1a
Ccr6
Nrp1
Cd44
Cd28
Nt5e
Pdcd1
Sell
Tcf7
Ccr7
WT_Naive subsets
WT_pre activaved subsets
WT_Klrg1+ subsets
WT_Gzmb+ subsets
WT_Nt5e+ subsets
WT_Tnfsf9+ subsets
WT_H2−Eb1+ subsets
WT_Mki67+ subsets
cKO_Naive subsets
cKO_pre activaved subsets
cKO_Klrg1+ subsets
cKO_Gzmb+ subsets
cKO_Nt5e+ subsets
cKO_Tnfsf9+ subsets
cKO_H2−Eb1+ subsets
cKO_Mki67+ subsets
G
Isotype
Foxp3cre
Foxp3creCxxc1fl/fl
CD4+YFP+
Count
CD25
CD69
ICOS
T-bet
CD25 MFI
CD69 (MFI)
ICOS MFI
T-bet MFI
H
CD4+YFP+
Lymph node
Foxp3cre
Foxp3creCxxc1fl/fl
CD4
IFN-γ
1.62
9.94
Percentage in CD4+YFP+(%)
I
Lymph node
Foxp3cre
Foxp3creCxxc1fl/fl
FOXP3
Ki-67
40.4
10.1
FOXP3+ Ki-67+(%)

Fig.6

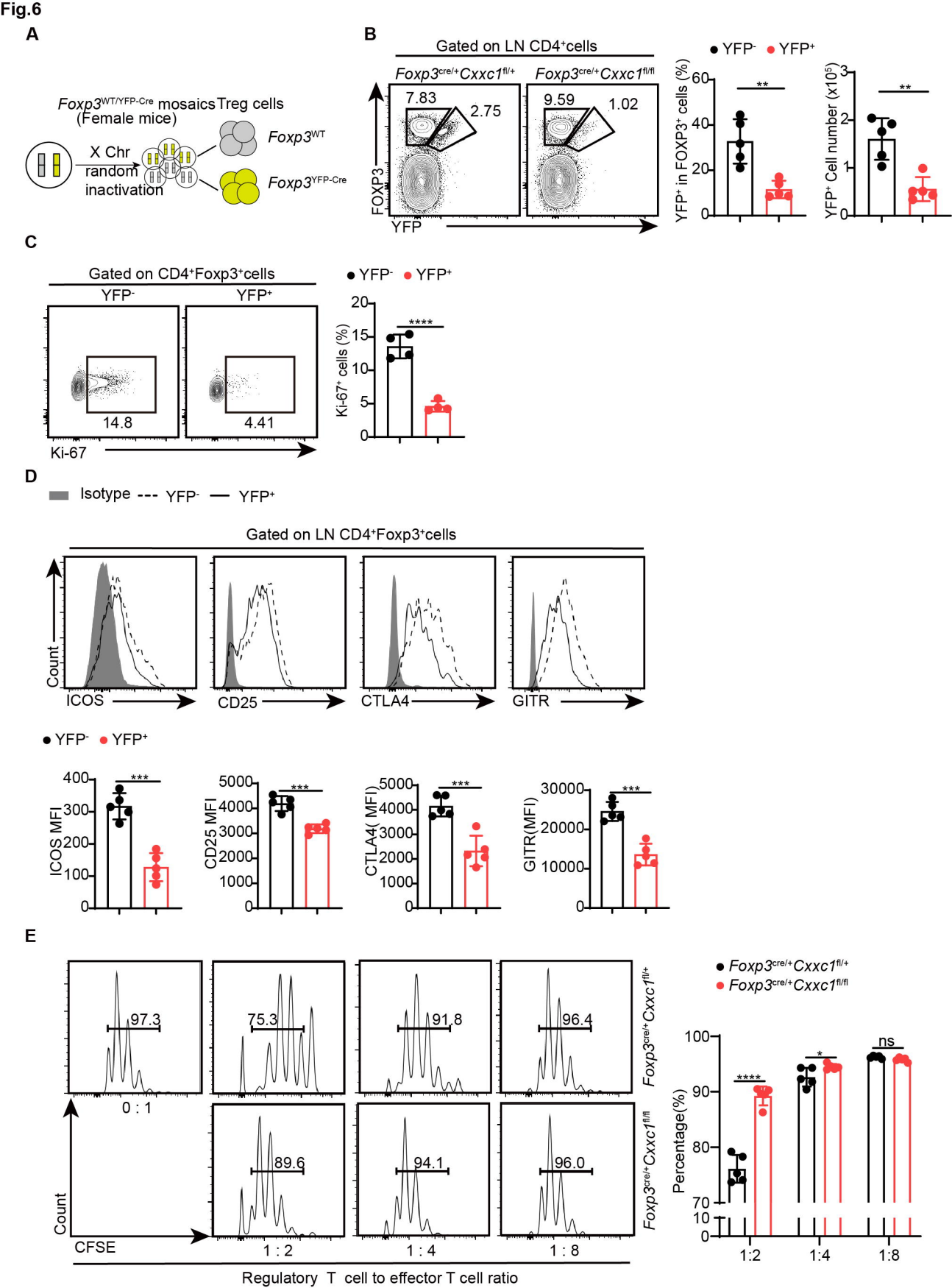
A
Foxp3WT/YFP-Cre mosaics Treg cells
(Female mice)
X Chr
random
inactivation
Foxp3WT
Foxp3YFP-Cre
B
Gated on LN CD4+cells
Foxp3cre/+Cxxc1fl/+
Foxp3cre/+Cxxc1fl/fl
7.83
2.75
9.59
1.02
FOXP3
YFP
YFP- YFP+
YFP+ in FOXP3+ cells (%)
YFP+ Cell number (x10^5)
C
Gated on CD4+Foxp3+cells
YFP-
YFP+
14.8
4.41
Ki-67
Ki-67+ cells (%)
D
Isotype
YFP-
YFP+
Gated on LN CD4+Foxp3+cells
Count
ICOS
CD25
CTLA4
GITR
ICOS MFI
CD25 MFI
CTLA4(MFI)
GITR(MFI)
E
97.3
75.3
91.8
96.4
89.6
94.1
96.0
0 : 1
1 : 2
1 : 4
1 : 8
Count
CFSE
Foxp3cre/+Cxxc1fl/+
Foxp3cre/+Cxxc1fl/fl
Percentage(%)
ns
1:2
1:4
1:8
Regulatory T cell to effector T cell ratio

Fig.7

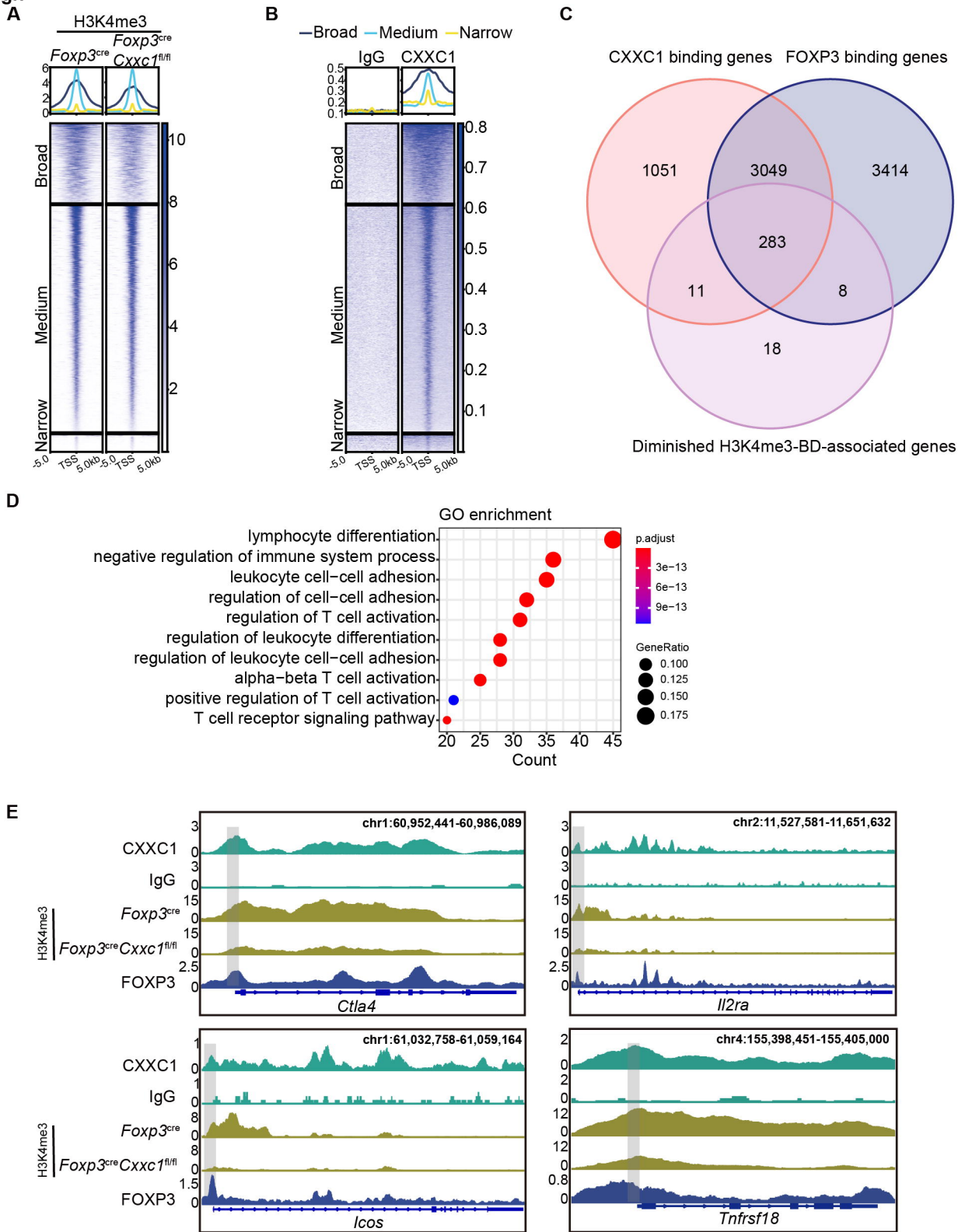
A
H3K4me3
Foxp3cre
Foxp3cre Cxxc1fl/fl
Broad
Medium
Narrow
-5.0
TSS
5.0kb
B
Broad
Medium
Narrow
IgG
CXXC1
C
CXXC1 binding genes
FOXP3 binding genes
Diminished H3K4me3-BD-associated genes
1051
3049
3414
283
11
8
18
D
GO enrichment
lymphocyte differentiation
negative regulation of immune system process
leukocyte cell−cell adhesion
regulation of cell−cell adhesion
regulation of T cell activation
regulation of leukocyte differentiation
regulation of leukocyte cell−cell adhesion
alpha−beta T cell activation
positive regulation of T cell activation
T cell receptor signaling pathway
Count
p.adjust
3e−13
6e−13
9e−13
GeneRatio
0.100
0.125
0.150
0.175
E
chr1:60,952,441-60,986,089
chr2:11,527,581-11,651,632
chr1:61,032,758-61,059,164
chr4:155,398,451-155,405,000
CXXC1
IgG
Foxp3cre
Foxp3cre Cxxc1fl/fl
FOXP3
H3K4me3
Ctla4
Il2ra
Icos
Tnfrsf18

Supplementary Figure 1

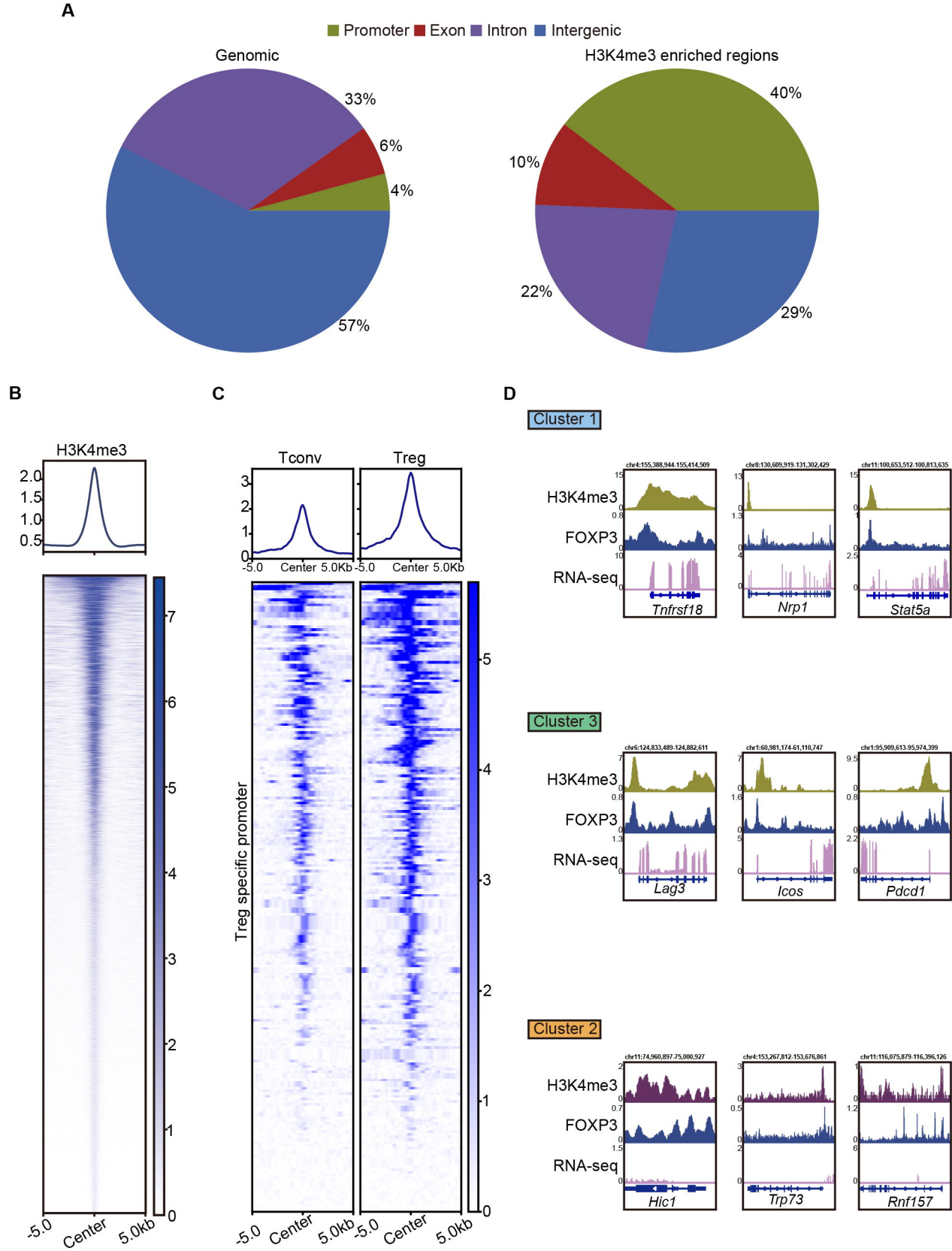

Supplementary Figure 2

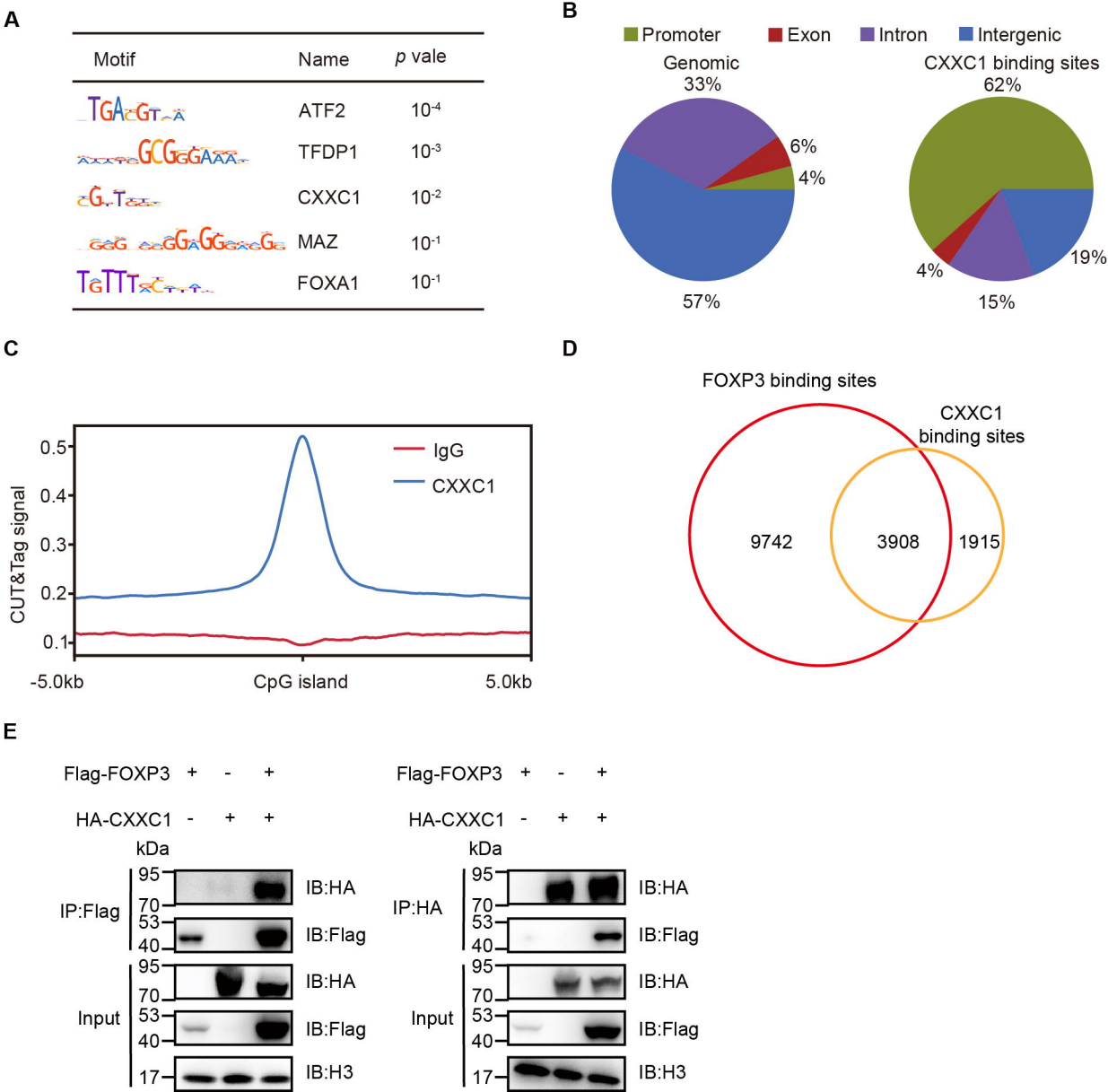

Supplementary Figure 3

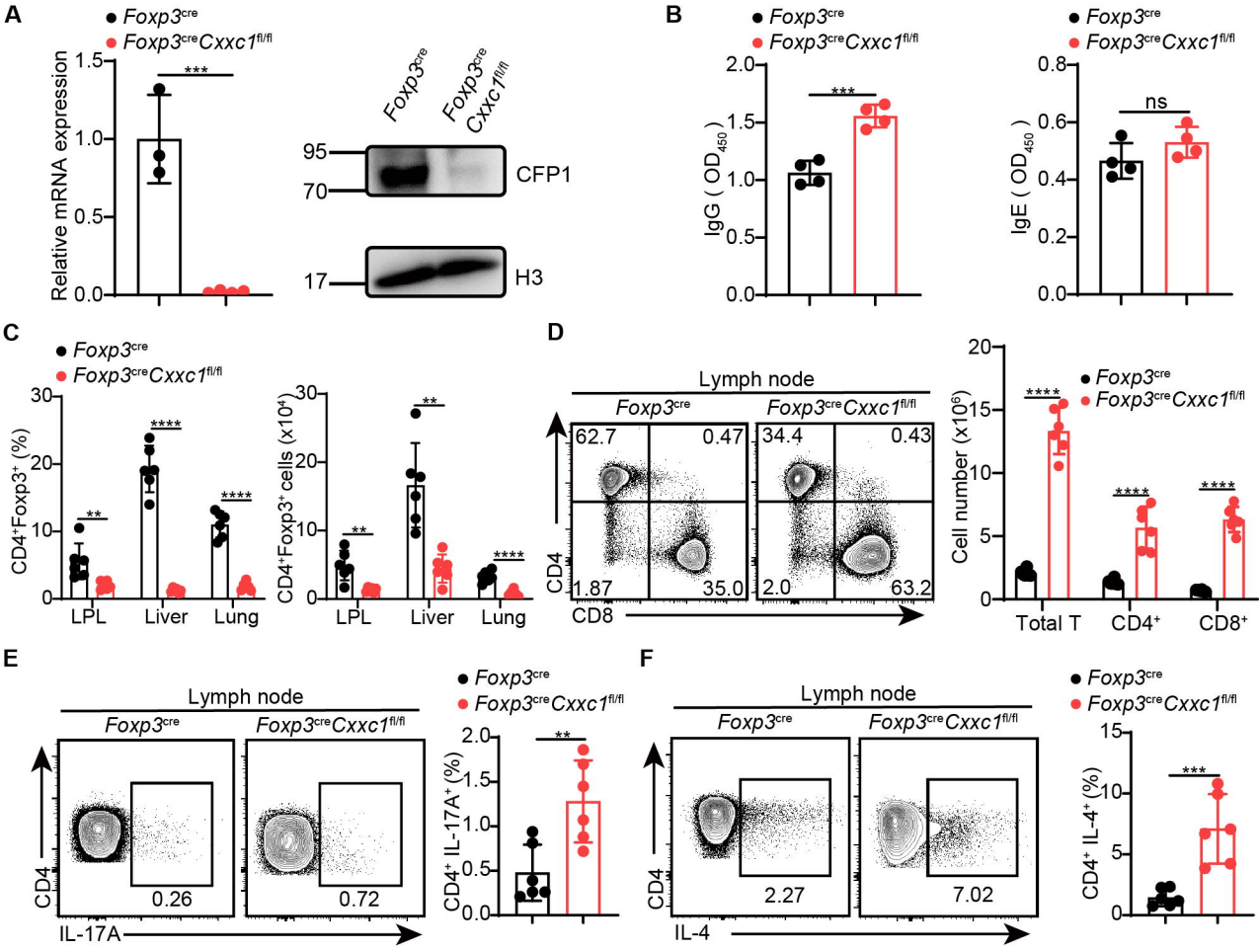

Supplementary Figure 4

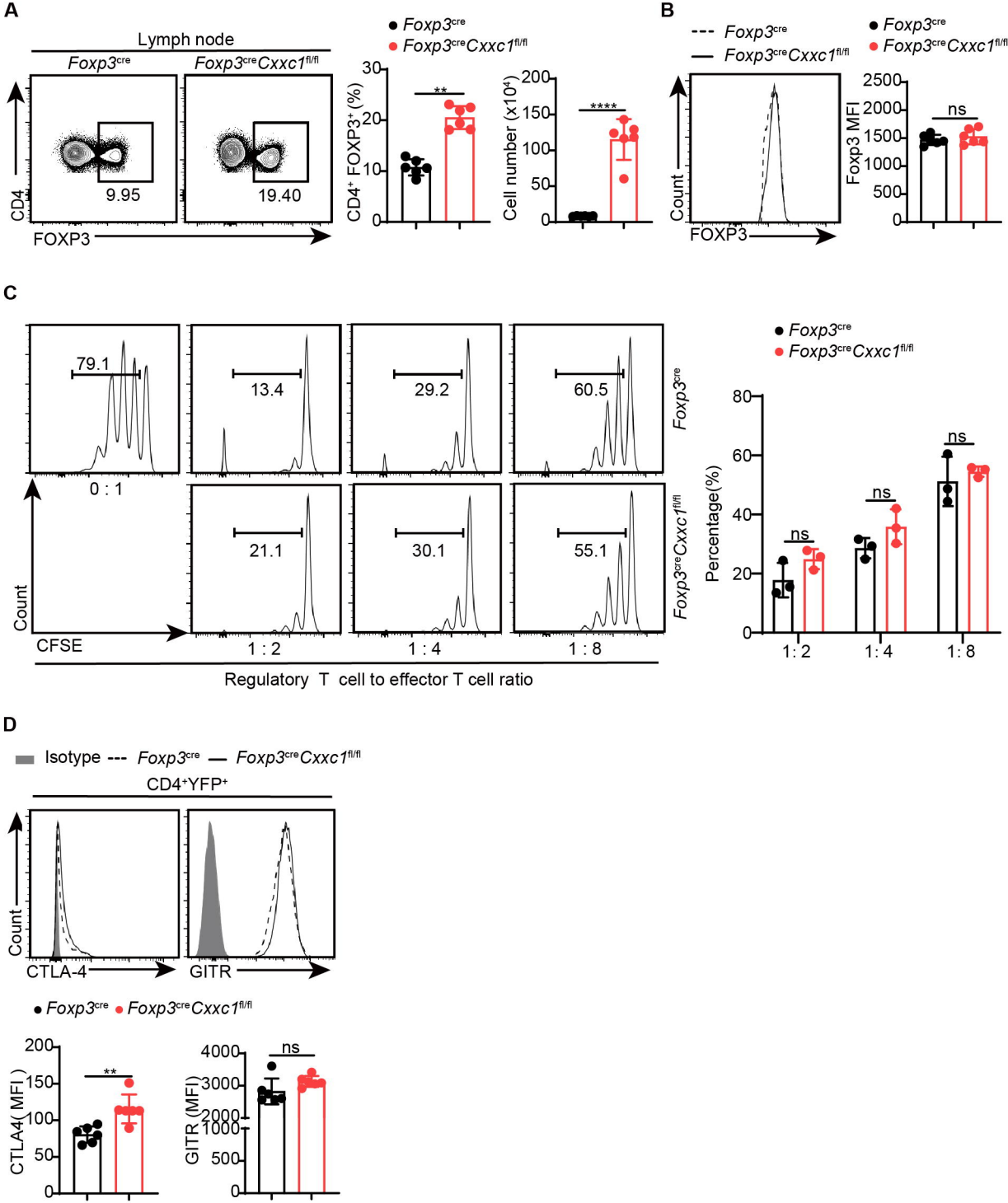

Supplementary Figure 5

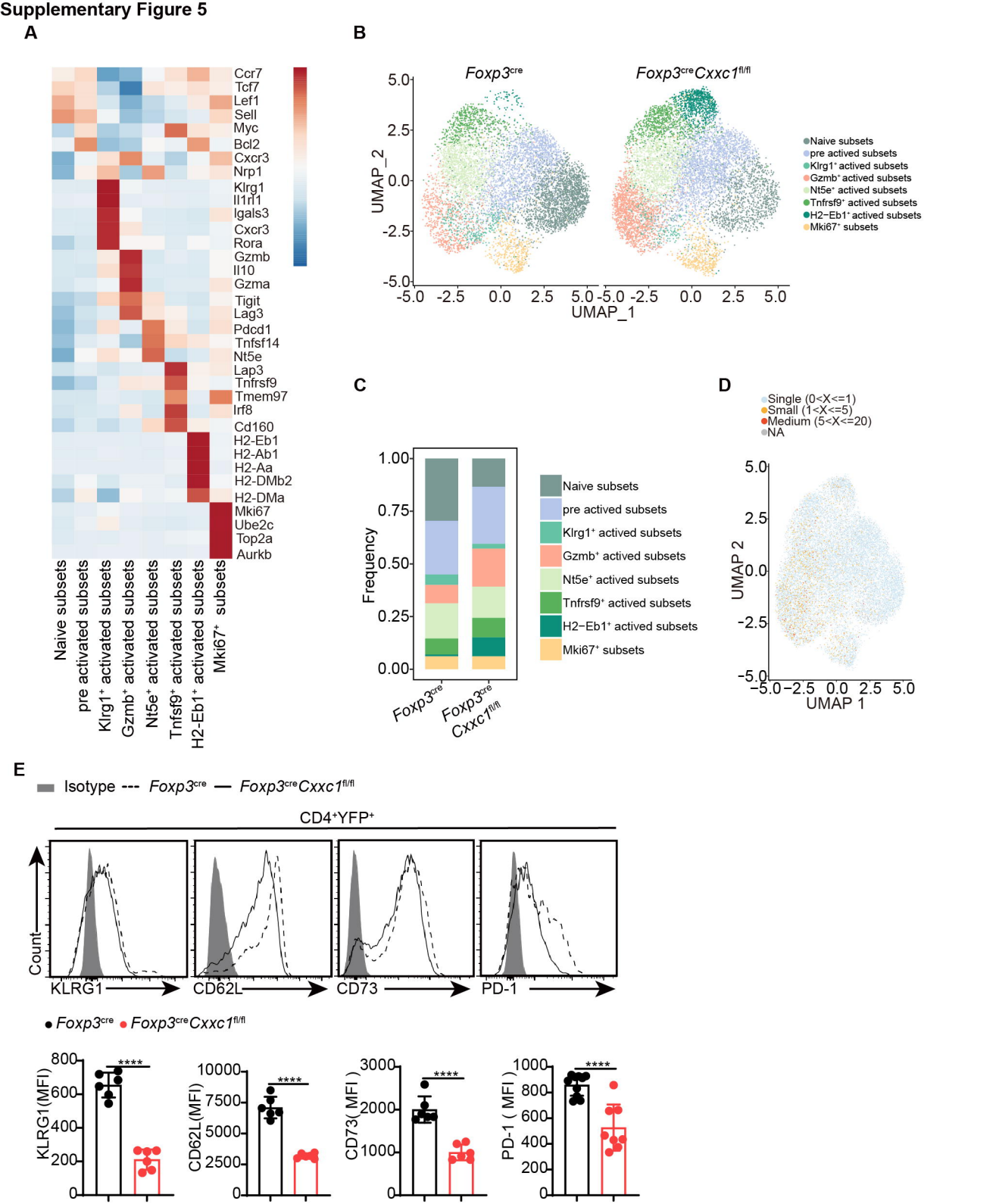

Supplementary Figure 6

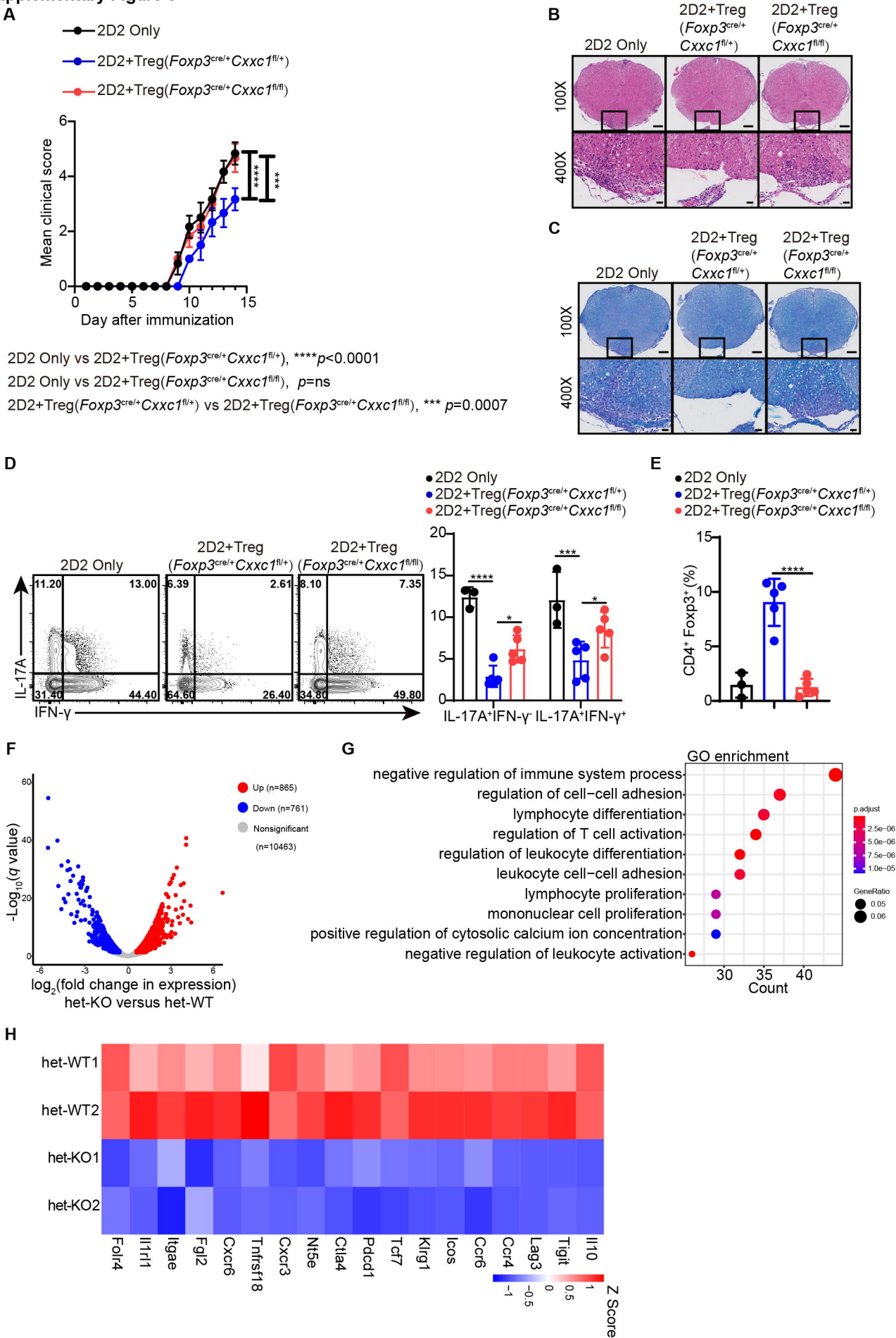

Supplementary Figure 7

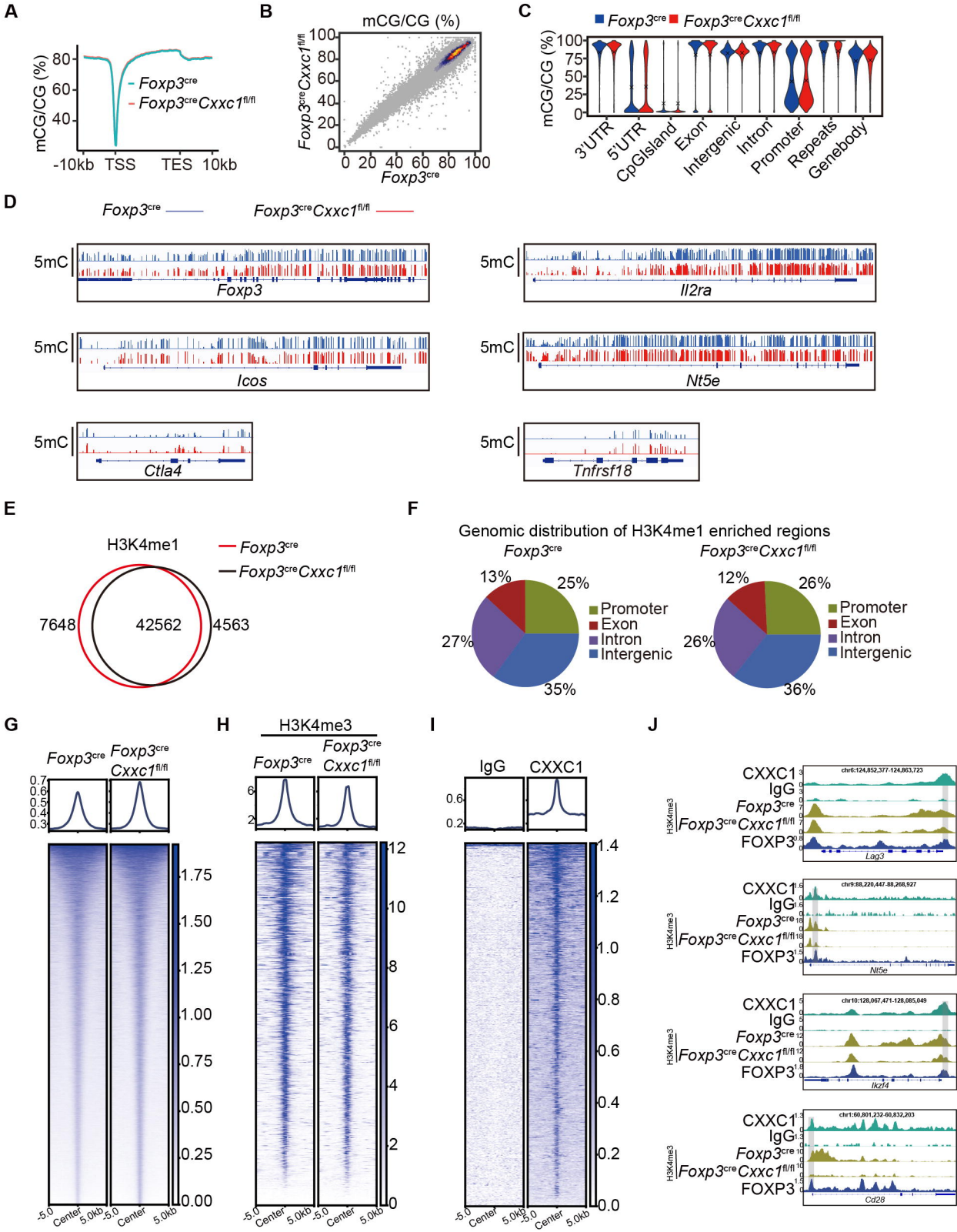
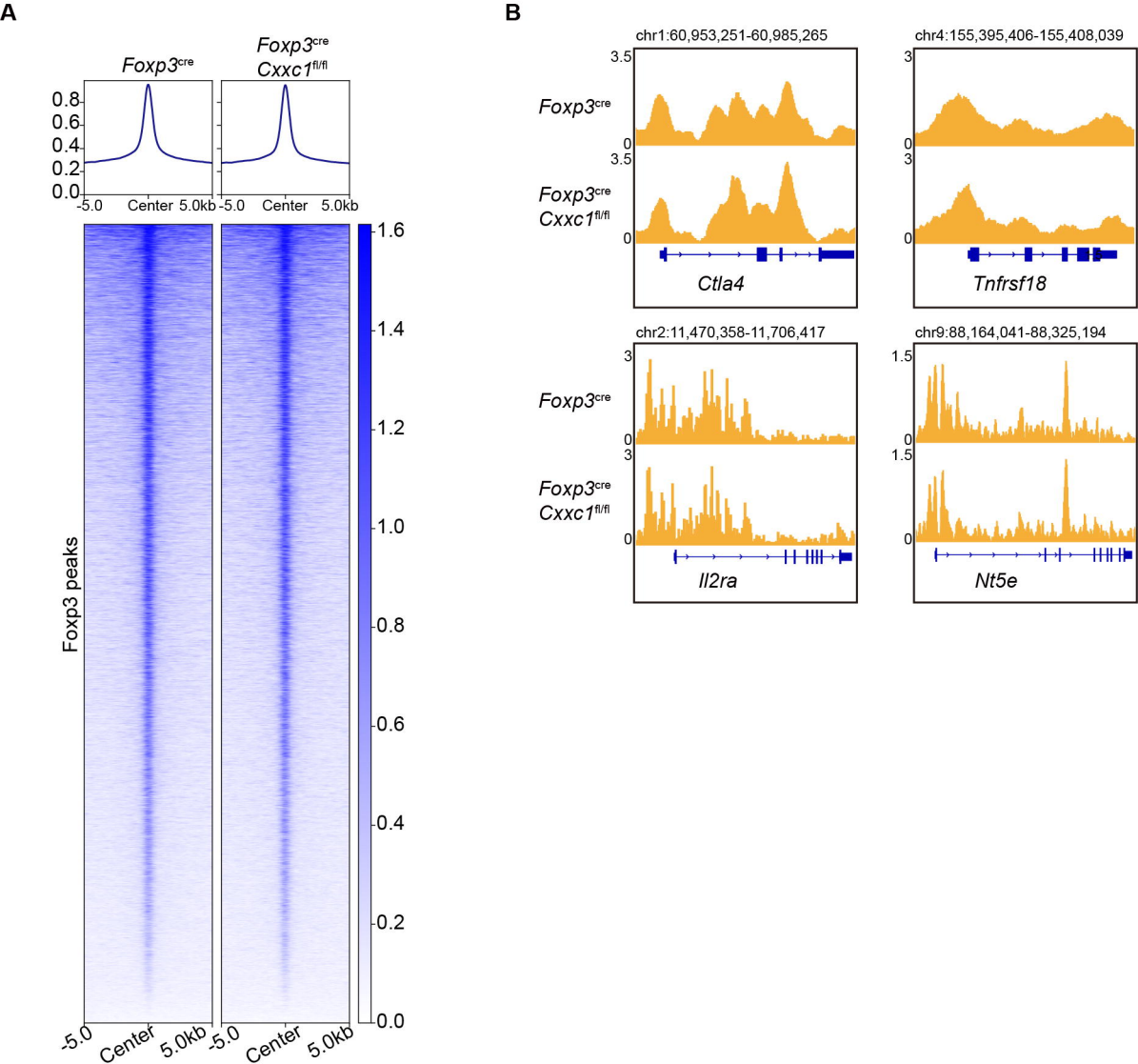
Supplementary Figure 8